Using salt cocrystals to improve the solubility of niclosamide

Using Salt Co-Crystals to Improve the Solubility of Niclosamide

Francesca Grifasi,[†] Michele R. Chierotti,[†] Katia Gaglioti,[†] Roberto Gobetto,[†] Lucia Maini,[‡] Dario Braga,[‡] Elena Dichiarante,[§] and Marco Curzi[§]*

† Dipartimento di Chimica I.F.M., Università di Torino, Via Giuria 7, 10125 Torino, Italy

‡ Dipartimento di Chimica G. Ciamician, Universitàdegli Studi di Bologna, Via Selmi 2, 40126 Bologna, Italy

§ PolyCrystalLine s.r.l., via F. S. Fabri 127/1, 40059 Medicina, Italy

KEYWORDS. Salt cocrystal, inorganic co-former, niclosamide, hydrogen bond, solid-state characterization, intrinsic dissolution rate, solid-state NMR

ABSTRACT. This communication sees us report the solvent-free synthesis and characterization of a number of different crystal forms of niclosamide (HNic), which is an API belonging to the Salicilamide class. The synthesized compounds are four new salt co-crystals (**KNic·HNic·H_2O**, **KNic·HNic·$3H_2O$**, **NaNic·HNic·$3H_2O$**, **NaNic·HNic·$2H_2O$**, a classic co-crystal with imidazole

(IM) (**HNic·IM**) and two sodium salts, (**NaNic·DMSO·H_2O** and **NaNic·DMSO·$2H_2O$**). The peculiarity of these salt co-crystals is the API's concomitant presence as both a neutral component and as a salt co-former and the fact that they interact via hydrogen bond formation. HNic's poor aqueous solubility makes the enhancement of its dissolution rate via the modulation of its physical properties extremely important. All samples have been investigated using a combination of solid-state experimental techniques which provide complementary information on powdered samples. These techniques are X-Ray Powder Diffraction, solid-state NMR, IR and Raman. Single crystals were only obtained for **KNic·HNic·H_2O** and **NaNic·DMSO·$2H_2O$**. The nature of the adducts (whether salt or co-crystal), their stoichiometry and the presence of independent molecules in the unit cell of the other samples were thus all determined by means of solid-state NMR and the comparative analysis of ^{13}C and ^{15}N CPMAS (Cross Polarization Magic Angle Spinning) and ^{1}H MAS spectra. Furthermore, differential scanning calorimetry, thermo-gravimetric analysis, intrinsic dissolution rate measurements completed the characterization and enabled us to evaluate the effects of microscopic changes (molecular packing, weak interactions, conformations, etc) on the macroscopic properties (thermal stability and bioavailability) of the multicomponent forms. The results obtained indicate that the formation of salt co-crystals provides a reliable method with which to improve the HNic intrinsic dissolution rate.

INTRODUCTION

Physicochemical property modulation is a remarkable means by which one can improve the features of a molecule and facilitate its use in many industrial application fields, from agriculture to pharmaceuticals. Due to a lack of required biopharmaceutical properties, less than 1% of API (Active Pharmaceutical Ingredient) appear on the marketplace.[1] Solubility is one of these key issues in pharmaceutical enforceability.[2] Despite offering potential improvements in flowability, chemical and physical stability and hygroscopicity, the design of pharmaceutical co-crystals has emerged as a potential method for enhancing the bioavailability of drugs with low aqueous solubility, thus increasing their intrinsic dissolution rate which is currently one of the main challenges for the pharmaceutical industry.[3]

Many approaches have been described for improving drug solubility, including salt formation,[4] emulsification,[5] solubilisation using co-solvents,[6] and the use of polymer drug vehicles for delivery.[7,8] Co-crystal design is a groundbreaking approach. Indeed, co-crystals are a reliable tool which to allow scientists to efficiently work on molecules without changing their efficacy, especially in pharmaceutical research.[9,10] These multi-component systems can be manipulated using crystal engineering,[11,12,13] via a supramolecular approach.

Co-formers usually are organic molecules in co-crystal design. However, co-former choice has recently expanded with the introduction of inorganic salts and the formation of ionic co-crystals,[14] where the neutral organic molecule directly interacts with alkali or alkaline-earth metals of halides, phosphate, sulphate salts. A further class of co-crystal can be found in salt co-crystals which are composed of the target neutral molecule and its molecular salt.[15] Molecular packing will be driven by the formation of hydrogen bonds and electrostatic interactions. This approach has the advantage

that both co-formers are the same chemical entity in solution. We have recently reported the water solubility improvement of tolfenamic acid by salt co-crystal formation with sodium and potassium carbonates as a promising strategy for pharmaceutical applications.[16]

Niclosamide (2,5-dichloro-4-nitrosalicylanilide, **Scheme 1**), hereafter HNic, is an API which belongs to the Salicilamide class and is the only commercially available antihelmintic for humans and animals to be recommended by the WHO (World Health Organization) for large scale use in schistosomiasis control programs. Significant potentiality as an anti-tuberculosis agent has also been observed.[17,18] One anhydrous and two different hydrate HNic forms have been reported in the literature. These have been labeled HNic, HNic Ha and HNic Hb, respectively, with HNic Hb being the most stable hydrate.[19] Furthermore, several co-crystals with caffeine, urea and theophylline,[20] have also been reported. HNic shows very poor aqueous solubility and as such belongs to Class II in the Biopharmaceutical Classification System (BCS), which includes compounds with high permeability and poor solubility. Therefore, the modulation of its physical and chemical properties (especially thermal stability and intrinsic dissolution rate) is clearly of great significance.

We herein report the solvent-free synthesis and solid state characterization of four new salt co-crystals (**KNic·HNic·H_2O**, **KNic·HNic·3H_2O**, **NaNic·HNic·3H_2O**, **NaNic·HNic·2H_2O**),[21] a classic co-crystal with imidazole (IM) (**HNic·IM**) and two salts of formula **NaNic·DMSO·H_2O** and **NaNic·DMSO·2H_2O**. The peculiarity of salt co-crystals is the concomitant presence of HNic both as a neutral component and as a salt co-former. Interestingly, the ionic co-former is obtained from HNic salification with an inorganic salt (i.e. sodium carbonate or potassium bicarbonate). The use of carbonates presents the advantage of the release of CO_2 and H_2O avoiding the presence of other salts in the final product.[22]

All samples were investigated using a combination of experimental solid-state techniques which provide complementary information on powdered samples.[23,24] These techniques are X-ray powder diffraction (XRPD), solid-state NMR (SSNMR), IR-ATR and Raman. Differential Scanning Calorimetry (DSC), Thermo-Gravimetric Analysis (TGA), and Intrinsic Dissolution Rate (IDR), measurements complete the characterization and the evaluation of crystal form dependent property modulation. The aim of this paper is to evaluate the ability of salt co-crystal formation to improve HNic performance (mainly in terms of thermal stability and bioavailability) as compared to classic co-crystals and salts which are the forms that pharmaceutical companies use the most.

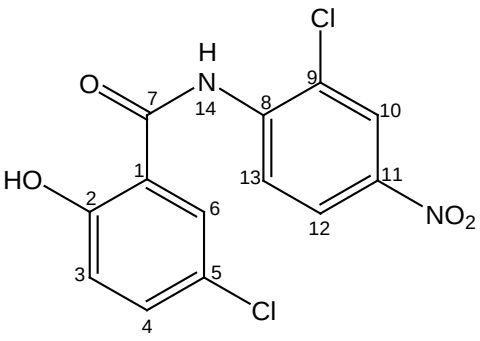

Scheme 1. HNic structure with numeration for SSNMR assignments.

EXPERIMENTAL SECTION

Materials and methods.

HNic was purchased from the Cayman Chemical Company (Japan) while all other reagents and solvents were purchased from Sigma-Aldrich and used without further purification. The HNic commercial batch was characterized by SSNMR analysis in the pure anhydrous form. The NaNic salt was prepared via the salification of 200 mg HNic with 6 ml NaOH solution (0.1M) in 40 ml of absolute ethanol at reflux temperature (80°C) for 3 hours. NaNic was obtained in a quantitative amount as a red powder which was found to be a polymorphic mixture. NaNic was the starting reagent for the synthesis of **NaNic·DMSO·2H_2O** and **NaNic·DMSO·H_2O** (see below).

Sample preparation.

Preparation procedures are summarized in **Table 1**. All samples were obtained using mechanochemical techniques, such as grinding or kneading (grinding with a catalytic amount (drops) of solvent).[25,26] All K and Na salt co-crystals were obtained using both bicarbonates and carbonates according to the appropriate stoichiometry. HNic Hb was produced according to the literature.[27]

KNic·HNic·H_2O; a quantitative amount of a yellow powder was obtained via the kneading (absolute ethanol) of HNic (200 mg) and potassium bicarbonate (30.6 mg) in a 2:1 stoichiometric ratio at room temperature for 25 minutes. It was also achieved by adding several drops of absolute ethanol to **KNic·HNic·3H_2O**. Orange, block shaped crystals, which are suitable for single crystal X-ray diffraction (XRSCD), were collected either via the slow, room temperature evaporation of a solution of a stoichiometric mixture of HNic and $KHCO_3$ (2:1) in hot ethanol (99.8%) or by recrystallizing the ground powder in absolute ethanol.

KNic·HNic·3H_2O; a quantitative amount of a red powder was obtained by kneading (ethanol/water 2:1) HNic (200 mg) and potassium bicarbonate (30.6 mg) in a 2:1stoichiometric

ratio at room temperature for 5 minutes. The sample, in powder form, was also collected by slow, room temperature evaporation of a solution which was obtained from dissolving a stoichiometric mixture (2:1) of HNic and $KHCO_3$ in a hot ethanol/water (2/1) mixture.

NaNic·HNic·2H₂O; a quantitative amount of a yellow powder was obtained by kneading (absolute ethanol) HNic (200 mg) and sodium carbonate (16.2 mg), in a 4:1 stoichiometric ratio, at room temperature for 35 minutes. It was also achieved by adding several drops of absolute ethanol to powdered **NaNic·HNic·3H₂O**.

NaNic·HNic·3H₂O; a quantitative amount of a red powder was obtained by kneading (ethanol/water 2:1) HNic (200 mg) and sodium carbonate (16.2 mg), in a 4:1 stoichiometric ratio, at room temperature for 5 minutes. The sample, in powder form, was also collected from the slow evaporation of a hot ethanol/water 2:1 solution of the reagents in a stoichiometric ratio 2:1.

HNic·IM; a quantitative amount of an orange powder was obtained by grinding HNic (200mg) and IM (41.6 mg) in a 1:1 stoichiometric ratio, at room temperature for 15 minutes.

NaNic·DMSO·2H₂O; a quantitative amount of a yellow powder was produced by kneading (DMSO) the NaNic polymorphic mixture (see above) for 5 minutes at room temperature. Pale yellow rectangular crystals, which are suitable for XRSCD analysis, were obtained from the slow room temperature evaporation of a solution which was obtained by dissolving the NaNic mixture in hot DMSO.

NaNic·DMSO·H₂O: a quantitative amount of a yellow powder was obtained by kneading (DMSO) the NaNic polymorphic mixture for 40 minutes (see above).

In all cases prolonged grinding does not lead to other transformations a part from a loss of crystallinity of the sample.

Table 1. Preparation procedures for **KNic·HNic·H_2O**, **KNic·HNic·3H_2O**, **NaNic·HNic·3H_2O**, **NaNic·HNic·2H_2O**, **HNic·IM**, **NaNic·DMSO·2H_2O** and **NaNic·DMSO·H_2O**. (g= grinding, k = kneading, cz= crystallization, s= seeding, p= powder, c= crystal)

Co-Formers		Preparation	Class	Formula	Form
HNic	$KHCO_3$	k, cz (EtOH 99%)	salt co-crystal	KNic·HNic·H_2O	yellow p, yellow block c
HNic	$KHCO_3$	k, cz (EtOH/H_2O 2:1)	salt co-crystal	KNic·HNic·3H_2O	red p, Red needle agglomerates
HNic	Na_2CO_3	k, cz (EtOH/H_2O 2:1)	salt co-crystal	NaNic HNic·3H_2O	brown p red needle agglomerates
HNic	Na_2CO_3	k (EtOH 99%)	salt co-crystal	NaNic·HNic·2H_2O	yellow p
HNic	IM	g	classic co-crystal	HNic·IM	bright orange p
HNic	NaOH	Salification reaction	Salt	Polymorphs mixture	brown p
NaNic Polymorphic mixture		k, cz (DMSO)	Salt	NaNic·DMSO·2H_2O	yellow p brown block c
NaNic Polymorphic mixture		k, s (DMSO)	Salt	NaNic·DMSO·H_2O	yellow p

Sample Characterization

X-ray diffraction. All crystal data were collected on an Oxford Xcalibur S instrument using Mo-Kα radiation (λ=0.71073 Å) and a graphite monochromator at room temperature. SHELX97 was used for structure solution and refinement and was based on F2.[28] Non-hydrogen atoms were

refined anisotropically. Carbon atom bound hydrogen atoms were added in calculated positions. Nitrogen atom bound hydrogen atoms were located using a Fourier map and their position refined. In structure **NaNic·DMSO·2H$_2$O,** the sulphur atom is disordered over two positions and was refined with occupancy values of 0.88 and 0.12. The hydrogen atoms bound to oxygen atoms were located from a Fourier map and their positions refined. In **KNic·HNic·H$_2$O,** the hydrogen atom bound to the HNic oxygen atom was added in calculated position for sake of clarity. It was not possible to locate the hydrogen atoms of the water molecule and they were omitted. Details of the crystal parameters for **KNic·HNic·H$_2$O** and the **NaNic·DMSO·2H$_2$O** salt are summarized in **Table 2**.

X-ray powder diffractograms were collected on a Panalytical X'Pert PRO automated diffractometer using Cu-Kα radiation and an X'Celerator detector without a monochromator, but which was equipped with an AntonPar TTK450 unit for controlled temperature measurements. The program PowderCell was used for the calculation of X-ray powder patterns on the basis of single-crystal data.[29]

Solid-state NMR measurements. All SSNMR spectra were recorded on a Bruker Avance II 400 instrument operating at 400.23, 100.65 and 40.55 MHz for ^{1}H, ^{13}C and ^{15}N nuclei, respectively. Cylindrical 4 mm o.d. zirconia rotors with a sample volume of 80 μL were used in ^{13}C and ^{15}N CPMAS spectra. Samples were spun at 12 and 9 kHz for ^{13}C and ^{15}N, respectively. A ramp cross-polarization pulse sequence was used with contact times of 3-5 (^{13}C) and 4 ms (^{15}N), a ^{1}H 90° pulse of 3.8-4 μs, recycle delays of 1-40 s and 95-3910 transients for ^{13}C and 860-15508 transients for ^{15}N. 2D ^{13}C-^{1}H FSLG (Frequency Switched Lee Goldburg) on- and off-resonance HETCOR spectra were measured according to the method described by van Rossum et al.[30] The MAS rate

was set to 12 kHz. The proton rf field strength used during the t_1 delay for FSLG decoupling and during TPPM acquisition (Two-Pulse Phase-Modulated) decoupling was 83 kHz. Two off-resonance pulses with opposite phases (i.e., +x, -x or +y, -y) during the FSLG decoupling were set to 9.8 μs in duration. The contact time used was 100 μs for the FSLG on-resonance CP HETCOR NMR spectrum. The magic angle (54.7°) pulse length for protons was set at 2.0 μs, while the recycle delay used was 15 s. Quadrature detection was achieved using the States-TPPI method. All the data for 64 t_1 increments, each of 140 scans, were collected. For the FSLG off-resonance CP HETCOR NMR spectrum, the intensity of the $B_1(^1H)$ field for the CP was 75 kHz, with a mixing period of 2.0 ms. The ^1H NMR chemical shift scale in the HETCOR spectra was corrected by a scaling factor of $1/\sqrt{3}$ because the ^1H NMR chemical-shift dispersion is scaled by a factor of $1/\sqrt{3}$ during FSLG decoupling.

^1H MAS experiments were performed on a 2.5 mm Bruker probe at a spinning speed of 32 kHz. The ^1H MAS spectra were acquired using the DEPTH sequence ($\pi/2–\pi–\pi$) to suppress the probe background signal.[31,32] The ^1H 90° pulse length was set to 2.50 μs, the recycle delays to 1-40 s and 32-64 transients were averaged for all samples. ^1H, ^{13}C and ^{15}N chemical shifts were referenced via the resonance of solid adamantane (^1H signal at 1.87 ppm), hexamethylbenzene (^{13}C methyl signal at 17.4 ppm) and $(NH_4)_2SO_4$ (^{15}N signal at -355.8 ppm with respect to CH_3NO_2).

Vibrational Spectroscopies. IR spectra were collected directly from the sample using a Harrick MVP2 ATR cell on a Bruker FT-IR Equinox 55 equipped with KBr optics and a DLaTGS detector. The spectra were acquired at 2 cm^{-1} resolution after 16-32 scans. Raman spectra were measured on a Bruker Vertex 70 spectrometer equipped with a RAM II using a 1064 nm Nd:YAG source and a Ge diode detector (laser power 10-50 mW, spectral resolution 4 cm^{-1}). IR and Raman spectra

were instrumental in the screening of products and monitoring preparations. In particular, attention was focused on the regions from 3500 to 3300 cm^{-1} (NH and OH stretching), 3100 and 3000 cm^{-1} (CH and CH_2 stretching) and 1700-1600 cm^{-1} (C=O stretching) in order to aid the identification of the different forms. All Raman and IR spectra are reported in the Supporting Information (**Figure S2** and **Figure S3**, respectively).

Calorimetric measurements. DSC analyses were performed on a TA instrument Q200. The samples (5-10 mg) were placed in closed aluminum pans and heated with a ramp of 10 °C min^{-1} in a temperature range of 30 to 400 °C.

TGA measurements were performed under N_2 flow (ramp, 10°Cmin^{-1}) on a TA instrument Q600 SDT Simultaneous DSC-TGA heat flow analyzer. The samples (5-10 mg) were placed in aluminum pans.

Intrinsic Dissolution Rate. Dissolution tests were performed on six different samples: HNic (commercial, anhydrous form), HNic Hb (the most stable hydrate form), **KNic·HNic·H_2O**, **KNic·HNic·$3H_2O$**, **NaNic·HNic·$2H_2O$** and **NaNic·HNic·$3H_2O$**. The extremely poor solubility of HNic in water meant that the IDR was measured in an EtOH/H_2O solution (1:1).

A calibration curve was constructed by plotting absorbance against concentration for five standard solutions of the sample in an EtOH/H_2O in standard concentrations The analyses were performed using a dissolution tester and methods described in "*European Pharmacopeia section 2.9.3 pg. 267*". The detector used was a UV-VIS Cary 50Varian equipped with an optic fiber. The program used was "*Concentration*" (Cary 50 WinUV Software V.3) and the measurement for each standard was recorded at 338 nm (for calibration curves and further details see **Figure S5** of the Supporting Information). The dissolution rates were performed on a Hanson's Vision Classic 6 dissolution

tester coupled with a Varian Cary 50 UV-Vis Spectrophotometer. The program used was "*Kinetic*" (Cary 50 WinUV Software V.3), which continuously recorded the absorbance of the solution at 338nm (80mL) under stirring (100rpm) at 37°C. The values obtained were converted from Abs/sec to g/sec and two measurements were recorded for each sample.

Each sample (approx. 100 mg) was compressed into a circular holder with a diameter of 3 mm, in order to standardize the contact surface between sample and media. The dissolution rate was calculated in the 10 and 60 seconds range, as all the samples presented a linear profile.

The HNic concentration during time (up to 72 h) of HNic co-crystals was evaluated using UV spectroscopy. A supersaturated solution (500 mg of powder in 40 ml of ethanol) of different samples was prepared and monitored for 72 h. A time-regular amount of solution was collected over the 72 hours and diluted with absolute EtOH to give the correct concentration for the analysis. Where a suspension was present, the sampled portion was centrifuged at 2000 rpm for one minute and the overlying solution was diluted with EtOH. All diluted samples were analyzed on a UV spectrometer. No data were acquired for the two salts **NaNic·DMSO·H_2O** and **NaNic·DMSO·$2H_2O$**, because of the small amount of sample obtained.

RESULTS AND DISCUSSION

Four new salt co-crystals, **KNic·HNic·H_2O**, **KNic·HNic·$3H_2O$**, **NaNic·HNic·$3H_2O$**, **NaNic·HNic·$2H_2O$**, have been synthesized via the mechanochemical (kneading) reaction of HNic with carbonates and bicarbonates (**Table 1**).

From the pharmaceutical point of view, the formation of salt co-crystals with carbonates presents several advantages as both co-formers are *de facto* the same chemical entity and thus have the same pharmacological activity. This avoids problems related to the type of co-former used, whether it is present in the pharmacopoeia as GRAS or not and gives relevant and evident advantages in patent issues. The US FDA has approved the sale of a salt co-crystal between valproic acid and its sodium salt as an anticonvulsant and mood-stabilizing drug, called Depakote®.[15] Carbonates or bicarbonates are also very effective reagents, even for pharmaceutical purposes, as they do not leave carbonate residues in the products because of CO_2 and H_2O evolution while grinding. HNic Hb, two sodium salts (**NaNic·DMSO·H_2O** and **NaNic·DMSO·$2H_2O$)** as well as a classic co-crystal **HNic·IM** were also obtained in order to compare their chemical physical properties with those of the achieved salt co-crystals.19 However, IM is not used for pharmaceutical purposes as it is, due to its high toxicology (LD50 in pig= 760 mg/kg) and is only used as a drug precursor.[33]

KNic·HNic·H_2O and **NaNic·DMSO·$2H_2O$** were characterized by XRSCD. Any correlation between XRSCD structures and bulk materials was checked by comparing calculated and measured diffraction patterns (**Figure S1** of the Supporting Information).

NaNic·HNic·$2H_2O$, **NaNic·HNic·$3H_2O$, KNic·HNic·H_2O** and **KNic·HNic·$3H_2O$** are hydrates and they differ only in hydration degree (**Table 1**). All these crystal forms are stable at ambient conditions for several weeks.

All salt co-crystals were subjected to dehydration thermal treatment (243 K for 30 min; ramp 2K/min) in vacuum in order to evaluate the hydration/dehydration process. In all cases, a mix of anhydrous polymorphs was obtained.

X Ray diffraction.

KNic·HNic·H_2O crystallizes as Triclinic P-1 and the asymmetric unit contains HNic, its potassium salt (KNic) and one water molecule. The structure is characterized by a HNic···Nic^- dimer formed via a very strong hydrogen bond of the type O-H···O^- (O···O distance= 2.447(7) Å) which is due to the cooperative effect of two other intramolecular N-H···O interactions (see **Figure 1**). This hydrogen bonding system, NH···O···H···O···HN, leads to the formation of the very strong $(C\text{-}O\cdots H\cdots O\text{-}C)^-$ interaction which resembles a single-well hydrogen bond, where the charge is equally distributed on both molecules. The co-crystal can thus be described as a salt between a $(Nic\cdots Nic)^-$ dimer (the anion) and K^+ (the cation). The potassium has a distorted octahedral coordination, five of the six oxygen atoms involved belong to the nitro and amide groups of five different molecules and sixth position is occupied by a single water molecule.

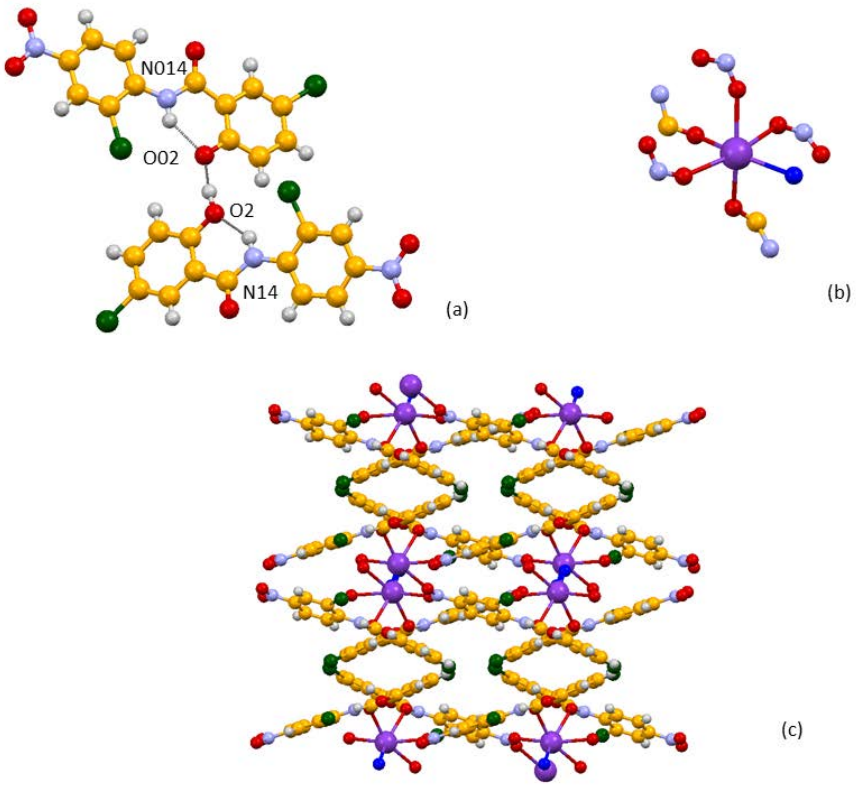

Figure 1. Crystal structure of **KNic·HNic·H$_2$O**: (a) short hydrogen bond between the HNic and Nic$^-$ forming the dimer; (b) potassium coordination (potassium in violet, oxygen in red, oxygen from water molecule in blue); (c) packing view along c axis.

NaNic·DMSO·2H$_2$O crystallizes as an orthorhombic; the sodium cation and the HNic lie on the mirror plane as well as the sulphur and oxygen atoms of the DMSO molecule, while the water molecule is in a general position. The coordination of the sodium atom is a distorted octahedral, where the equatorial positions are occupied by the water molecules, while the axial ones are occupied by the oxygen of the amide group and by one chlorine atom. The deprotonated hydroxyl group is involved in a short intramolecular N-H···O$^-$ hydrogen bond (2.573(4) Å) and two O$_w$-H···O$^-$ contacts with two adjacent water molecules (**Figure 2b**).

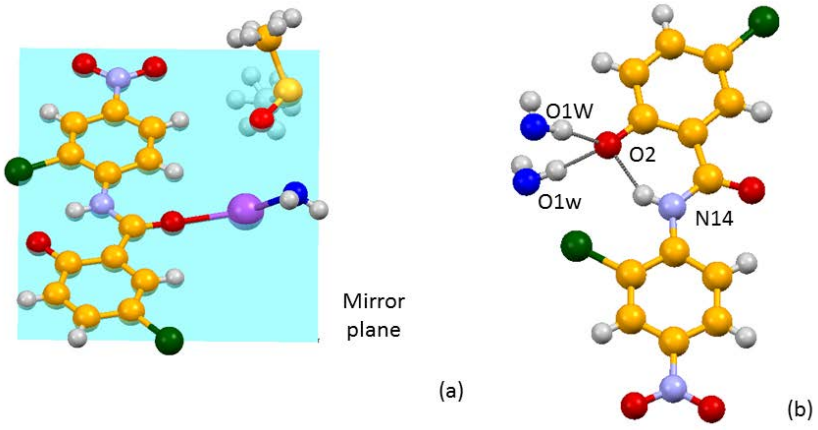

Figure 2. Asymmetric unit of **NaNic·DMSO·2H$_2$O** with the molecule of Nic$^-$ and the Na$^+$lying on the mirror plane (in light blue) as well as the sulphur and the oxygen of the DMSO molecule. Only the methyl group of DMSO and the water molecule are in general position. The disordered position of the sulphur is omitted for sake of clarity (a).The hydrogen bonds involving the deprotonated hydroxyl group (b). [Purple, light-blue, orange, white, red, green and yellow spheres represent potassium, nitrogen, carbon, hydrogen, oxygen, chlorine and sulphur atoms, respectively, Oxygem atoms of water molecules are represented in blue]

Since the Nic$^-$ lies on the mirror plane, packing is characterized by the presence of layers. Each water molecule bridges two sodium cations and donates two hydrogen bonds to Nic$^-$ and DMSO. Overall packing is shown in **Figure 3**.

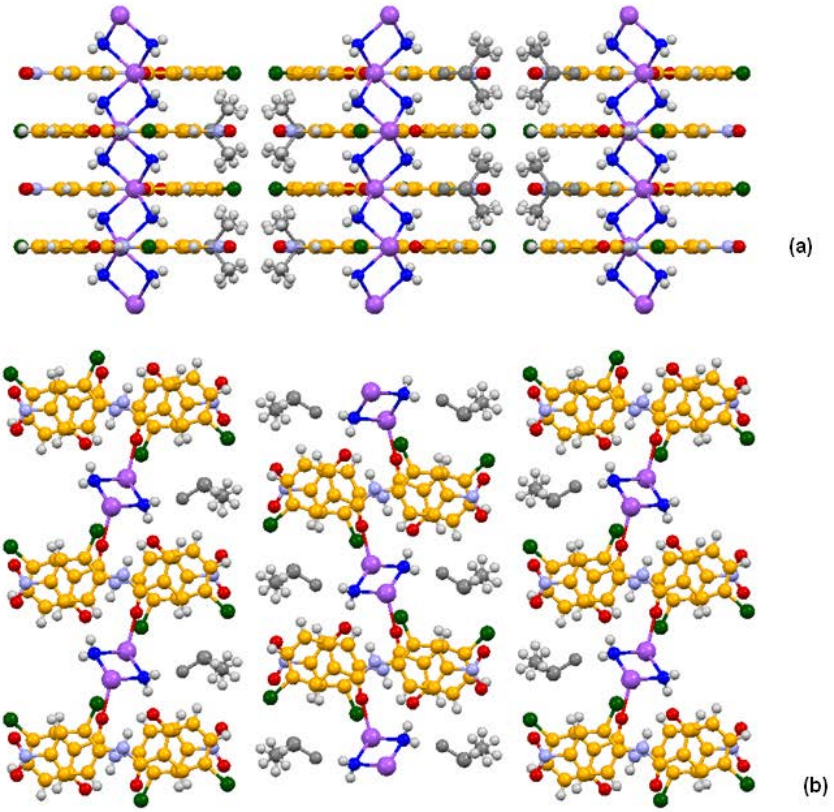

Figure 3. Molecules of **NaNic·DMSO·2H$_2$O** along the a axes (a) and the c axes (b). DMSO molecules are represented in light grey and water molecules in blue.

Crystal data, relevant hydrogen bonds and other interatomic distances are reported in **Table 2** and **Table 3**.

It is worth noting that HNic is characterized by a near planar conformation in pure HNic and in all reported structures due to an intramolecular N-H···O$_{intra}$ hydrogen bond.

Table 2. Crystal data for the salt co-crystal **KNic·HNic·H$_2$O** and for the salt **NaNic·DMSO·2H$_2$O**.

	KNic·HNic·H$_2$O	**NaNic·DMSO·2H$_2$O**
formula	$C_{26}H_{17}N_4Cl_4K_1O_9$	$C_{15}H_{17}Cl_2N_2NaO_7S$
space group	P-1	P n a m
a (Å)	10.006(2)	9.9203(6)
b (Å)	10.928(3)	29.859(3)
c (Å)	13.135(3)	6.7512(8)
α (deg.)	97.36(2)	90
β (deg.)	90.05(2)	90
γ (deg.)	93.93(2)	90
V (Å^3)	1421.01	1999.77
Z,Z'	Z= 2; Z'= 1	Z= 8; Z'= 0.5
R%	8.68	8.91

Table 3. Selected hydrogen bond and carbonyl distances as obtained from **KNic·HNic·H$_2$O** and **NaNic·DMSO·2H$_2$O** crystal data.

Sample	**Label**	**Distance (Å)**
KNic·HNic·H$_2$O	$N_{14}(-H_{14})\cdots O_2$	2.583(7)
	$N_{014}(-H_{014})\cdots O_{02}$	2.615(7)
	$O_2(-H_2)\cdots O_{02}$	2.477(7)
	$O_{02}\cdots O_{1w}$	2.925(7)
	$C_7=O_7$	1.222(7)
	$C_{07}=O_{07}$	1.237(7)
	$C_2-O_2(H_2)$	1.321(8)
	$C_{02}-O_{02}^-$	1.314(8)
NaNic·DMSO·2H$_2$O	$N_{14}(-H_{14})\cdots O_2$	2.573(5)
	$O_{1w}(H_{101})\cdots O_2$	2.747(4)
	$O_{1w}(H_{100})\cdots O_{10}$	2.822(4)
	C_2-O_2	1.298(6)
	$C_7=O_7$	1.246(6)

Solid-state NMR characterization

The structure and packing profiles of the compounds whose crystals were not suitable for XRSCD, were deducted from SSNMR data in analogy with those of **KNic·Nic·H_2O** and **NaNic·DMSO·$2H_2O$**.

All ^{1}H and ^{13}C chemical shifts and assignments are reported in **Table 4** whereas the ^{13}C CPMAS and ^{1}H MAS spectra are reported in **Figures 4** and **Figure 5**, respectively. ^{1}H-^{13}C FSLG on and off-resonance CP HETCOR (**Figure 6**) and ^{15}N CPMAS (**Figure 7**) spectra were only necessary for **HNic·IM**. ^{15}N chemical shifts and assignments are reported in **Table 5**. For atom numbering, we refer the reader to **Scheme 1**.

Table 2. ^{1}H and ^{13}C chemical shifts with assignments for HNic, HNic Ha, HNic Hb, **KNic·HNic·H_2O, KNic·HNic·$3H_2O$, NaNic·HNic·$3H_2O$, NaNic·HNic·$2H_2O$, HNic·IM, NaNic·DMSO·$2H_2O$** and **NaNic·DMSO·H_2O**.

Note	n	HNic	HNic Ha	HNic Hb	KNic·HNic ·H_2O	KNic·HNic ·$3H_2O$	NaNic·HNic ·$3H_2O$	NaNic·HNic ·$2H_2O$	HNic·IM	NaNic·DMSO ·$2H_2O$	NaNic·DMSO ·H_2O
							^{13}C CPMAS				
C-NO_2	11	143.3	143.8	141.8	144.2	145.1	144.6	144.1	143.0	142.2	142.1
CH_{Ar}	3, 4, 6, 10, 12, 13	136.1 130.3 125.7 119.7	134.9 128.6 122.9 118.7	135.0 130.8 122.7 119.3 117.9	133.5 131.4 124.9 121.2 119.1	133.9 128.6 122.4 121.0	133.7 128.5 123.1 120.2 121.8sh	133.6 131.9 124.2 123.5sh 120.6 118.7	124.5 120.6 121.2 129.9	128.9 125.1 120.5 116.6	127.9 125.5 123.9 119.1 118.1sh
C-Cl	5, 9	129.8sh 125.7	127.0sh 126.7sh	127.3sh 125.8	124.9 124.9	125.2	123.1 125.5	124.2 123.5sh 127.2	139.7	140.2	142.1
C-NH	8	139.9	141.3	140.3	139.9	139.8	139.9	141.9 140.6	124.5	130.5	132.2
C=O	7	162.9	164.0	162.7	163.1	164.3	164.4	165.3 168.5	166.3	165.2	167.2
C-CO	1	117.4	117.3	117.9	118.2sh	115.6	115.4	118.7	118.7	118.4	114.9
C-OH/C-O^-	2	153.9	155.0	154.6	167.1	167.3	167.8	168.5 161.6	161.6	167.6	168.8
CH_3	-	--	--	--	--	--	--	--	-	41.5	41.0, 40.3
	^{1}H MAS										
OH	2	10.7sh	11.6	11.6	18.5	18.5	18.4	18.7	18.2	--	--
H_{Ar}	3, 4, 6, 10, 12, 13	8.5-6.9sh	7.8	7.9	8.1-7.3	8.1-7.3	7.3-8.0	7.7	7.5	7.9, 6.5	7.9sh-6.5
NH	14	8.5-6.9sh	11.6	11.6	13.6	13.6	13.6	13.3	12.6	15.0	15.0
H_2O	-	--	4.0	4.6	4.3	4.3	4.1	3.3	--	2.9	2.9
CH_3	-	--	--	--	--	--	--	--	--	2.9	2.9
Z’		1	1	1	2	2	2	2	2	1	1

Z’ refers to independent Nic^- and/or HNic molecules.

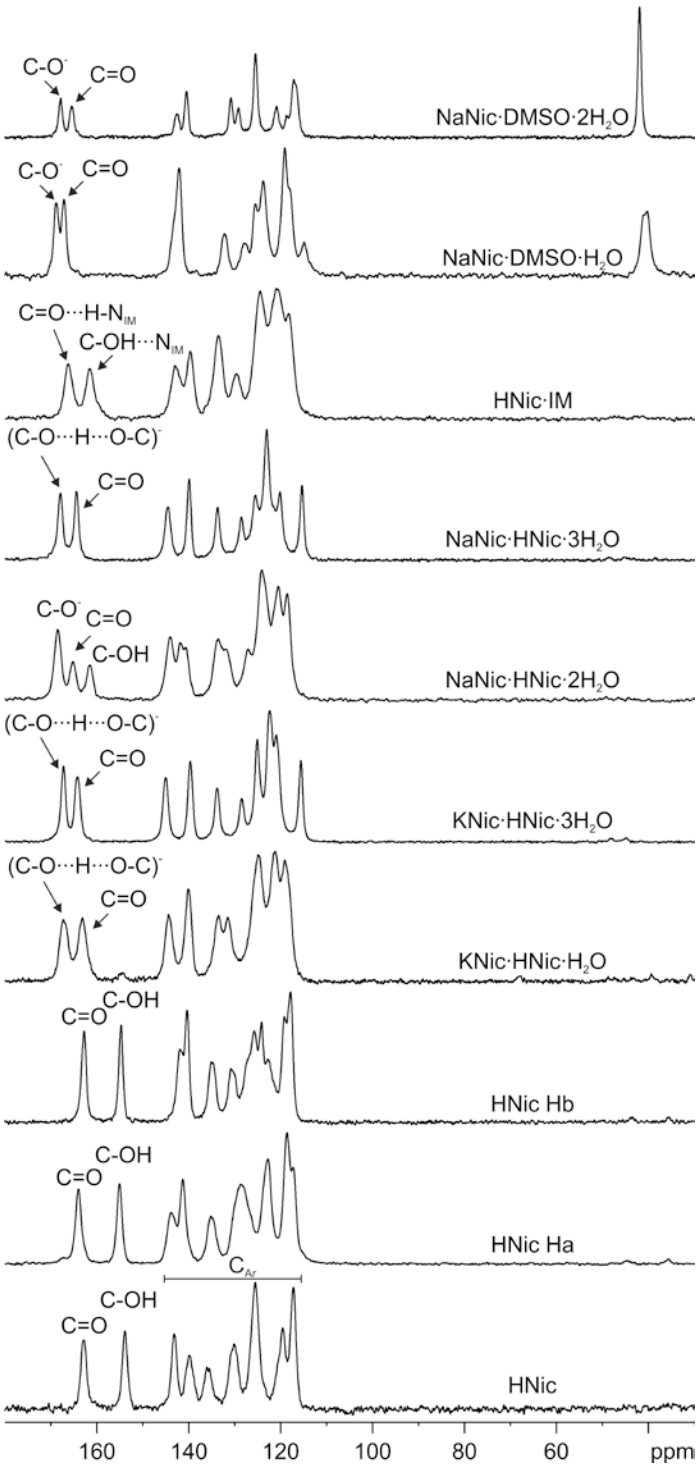

Figure 4. ^{13}C (100 MHz) CPMAS spectra with the relevant assignments of HNic, HNic Ha, HNic Hb, **KNic·HNic·H2O**, **KNic·HNic·3H2O**, **NaNic·HNic·3H2O**, **NaNic·HNic·2H2O**, **HNic·IM**, **NaNic·DMSO·2H2O** and **NaNic·DMSO·H2O**, recorded at 12 kHz.

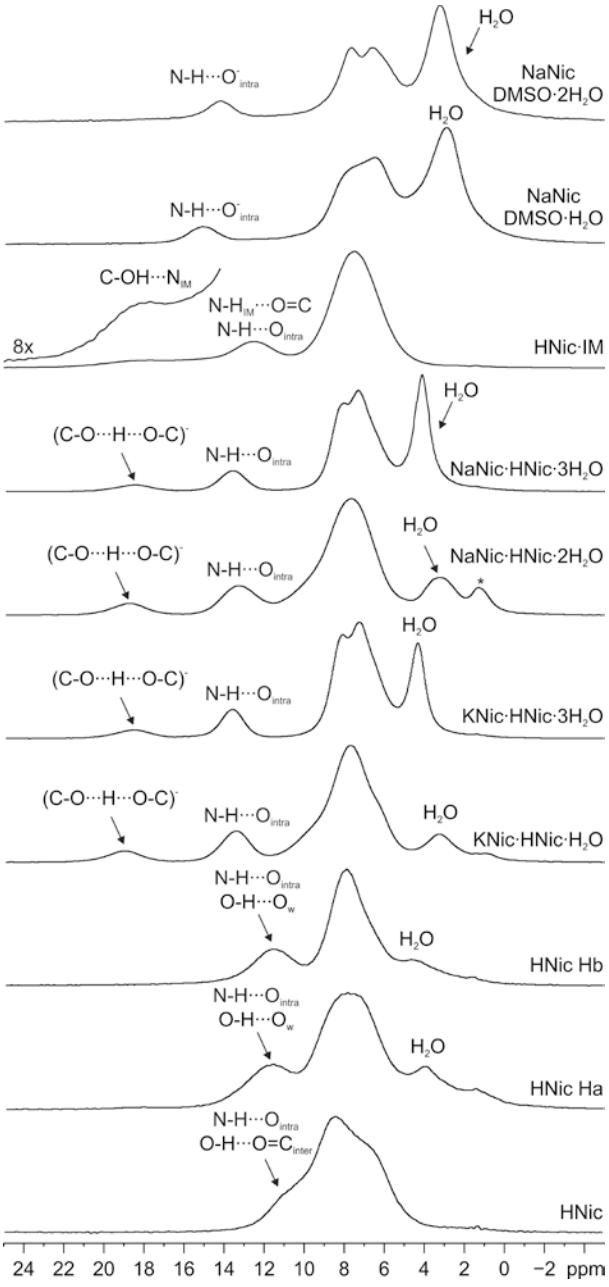

Figure 5. ^{1}H (400 MHz) MAS spectra with the relevant assignments of HNic, HNic Ha, HNic Hb, **KNic·HNic·H$_2$O**, **KNic·HNic·3H$_2$O**, **NaNic·HNic·3H$_2$O**, **NaNic·HNic·2H$_2$O**, **HNic·IM**, **NaNic·DMSO·2H$_2$O** and **NaNic·DMSO·H$_2$O**, recorded at 32 kHz. (The asterisk indicates an impurity).

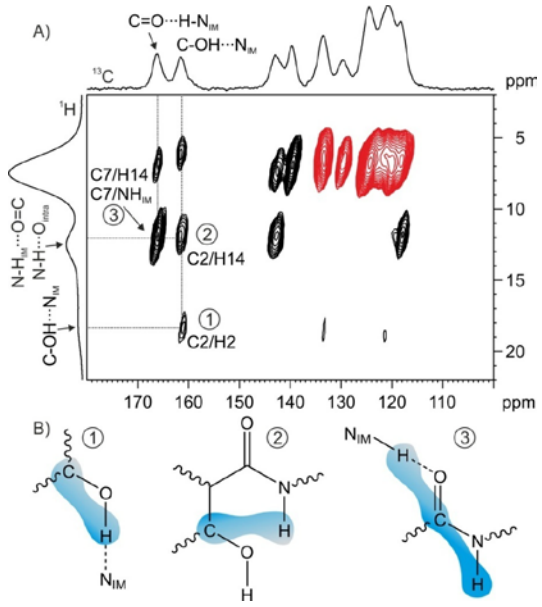

Figure 6. A) ^{1}H-^{13}C FSLG off-resonance CP HETCOR spectrum with the relevant assignments of **HNic·IM** acquired with a contact time of 1500 µs. (Red correlations peaks are those observed in the on-resonance CP HETCOR acquired with a contact time of 50); B) Schemes of the main ^{1}H-^{13}C proximities.

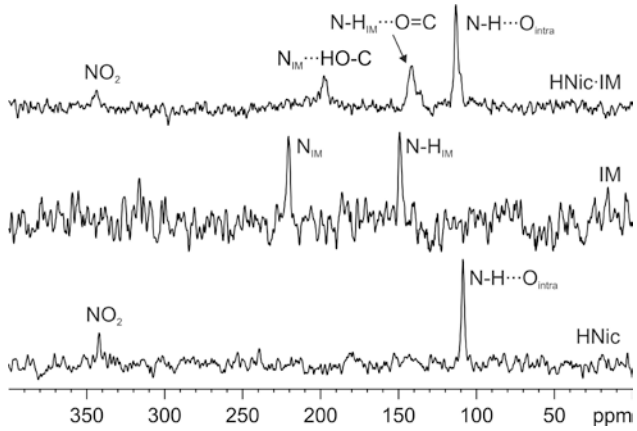

Figure 7. ^{15}N (40.56 Hz) CPMAS spectra with the relevant assignments of HNic, IM and **HNic·IM** recorded at 9 kHz.

Table 3. ^{15}N chemical shifts with assignments for pure HNic, pure IM and **HNic·IM**

$\delta^{15}N$	**HNic**	**IM**	**HNic·IM**
NH	108.7		112.4
NO_2	341.9		343.2
NH_{IM}		149.2	140.7
N_{IM}		220.5	195.8

The presence of a strong $(C\text{-}O\cdots H\cdots O\text{-}C)^-$ hydrogen bond in **KNic·HNic·H_2O** is confirmed by the ^1H MAS spectrum which is characterized by a peak at 18.5 ppm. Indeed, the high-frequency shift of the hydrogen-bonded atom (from 10.7 to 18.5 ppm) is directly related to the presence and the strength of the hydrogen bond.[34] The ^{13}C CPMAS spectrum of **KNic·HNic·H_2O** is characterized by a resonance at 167.1 ppm. This is attributed to the C-OH groups of both Nic^- and HNic which are involved in the strong $(C\text{-}O\cdots H\cdots O\text{-}C)^-$ interaction. The high-frequency shift of this signal from 153.9 ppm, in pure HNic, to about 167 ppm in the salt co-crystal accounts for the formation of this contact, where the charge is equally distributed along the whole $(C\text{-}O\cdots H\cdots O\text{-}C)^-$ system and the H2 hydrogen atom probably lies on the middle of the contact at room temperature or is mobile along the two positions on the NMR time scale. This causes the two independent molecules to be chemically very similar; in such a way the signal differences fall under the natural peak broadening and justify the presence of a single set of ^{13}C signals instead of the two sets expected given the crystallographic data.

A similar shift in the ^{13}C C-OH resonance was also observed in **NaNic·HNic·3H_2O**, **KNic·HNic·H_2O** and **KNic·HNic·3H_2O**. The presence of similar interactions can thus also be assumed for these samples. In this sense, **NaNic·HNic·2H_2O** is an exception. Indeed, the presence of two sets of signals indicates a lower chemical equivalence between the two molecules (HNic and Nic^-). Furthermore, the concomitant presence of a peak at 168.5 ppm (typical of a $C\text{-}O^-$) and

at 161.6 ppm (attributed to a C-OH) indicates the localization of the negative charge on only one molecule.

The ^{1}H peak, related to the (C-O···H···O-C)$^{-}$ hydrogen atom (**Figure 5**), shifts from 10.3 ppm (pure HNic) to about 18-19 ppm in all samples, confirming the presence of a very strong interaction. This is also observed in **NaNic·HNic·2H$_2$O** where the lack of hydrogen mobility or its asymmetric position along the contact probably decrease the symmetry of the two molecules. However, the ^{1}H signal around 11-15 ppm in all spectra confirms the presence of an intramolecular N-H···O hydrogen bond typical of HNic in all its crystal forms.

The ^{13}C CPMAS spectrum of **HNic·IM** suggests the formation of a co-crystal rather than a salt even though the classification remains ambiguous. The high-frequency shift of the HNic ^{13}C C-OH resonance from 153.9 ppm to 161.6 ppm suggests the formation of a strong hydrogen bond, in this case, with the IM tertiary nitrogen atom (N_{IM}). On the other hand, the ^{13}C C=O resonance shifts from 162.9 (pure HNic) to 166.3 ppm indicating that the C=O is involved in a C=O·· HN_{IM} contact. The ^{15}N CPMAS spectrum also provides interesting results. The observed ^{15}N shift of around 20 ppm (from 220.5 to 195.8 ppm) is compatible with the formation of a strong C-OH·· N_{IM} interaction, since imidazolium formation is characterized by a ^{15}N low-frequency shift of N_{IM} of more than 40 ppm.[35] The presence of this strong contact is also confirmed by the ^{1}H MAS spectrum (**Figure 5**) which shows a signal at 18.2 ppm. Further evidence is provided by the ^{1}H-^{13}C FSLG off-resonance CP HETCOR spectrum (**Figure 6**) which shows polarization transfer from the ^{1}H signal at 18.2 ppm to the C2 (^{13}C δ=161.6). This means that H2 and C2 are closer than about 3 Å,[36] confirming the formation of a C-OH···N contact rather than C-O^{-}···H-N^{+}. Other main correlations involve the C7/NH_{IM} and C2/H14 atom pairs. The former confirms the formation of the C=O·· HN_{IM} interaction while the latter the presence of the intramolecular N-H···O hydrogen

bond, which is typical of HNic. Other IM ^{13}C and ^{1}H peaks fall under the HNic signals preventing any further information (^{13}C signals in the range 139-120 ppm and ^{1}H N-H_{IM} peak overlapped with the HNic N-H at 12.5 ppm).

NaNic·DMSO·2H_2O salt formation is confirmed by the presence of a signal at 167.6 ppm which is typical of C-O^- groups ($\delta_{C\text{-}OH}$ HNic= 153.9 ppm). The ^{13}C spectrum (Figure 4) is also characterized by a signal at 41.5 ppm that indicates the occurrence of a DMSO molecule. The ^{1}H MAS spectrum (Figure 5) shows a moderate intramolecular N-H···O^- hydrogen bond (signal at 15.0 ppm) and the integration of ^{1}H peaks confirms the presence of two water molecules in the unit cell.

NaNic·DMSO·H_2O salt formation is confirmed by the signal at 168.8 ppm which is typical of C-O^- groups ($\delta_{C\text{-}OH}$ HNic= 153.9 ppm), while the CH_3 groups of DMSO fall at 41.0 and 40.3 ppm indicating a lower molecule symmetry than the dihydrated form. In the ^{1}H MAS spectrum (Figure 5), the peak at 15.0 ppm indicates a moderate intramolecular N-H···O^- hydrogen bond. The presence of one molecule of DMSO and one molecule of H_2O is confirmed by combining the integration of ^{1}H MAS peaks with TGA data.

Differential Scanning Calorimetry and Thermogravimetric Analyses.

The water uptake/release process was studied by means of calorimetric methods in order to investigate the possibility of achieving anhydrous salt co-crystals. All results are reported in **Table 6**. All DSC and TGA figures are reported in the Supporting Information.

Upon heating, the salt co-crystals release structural water at around 94 to 113°C. In all cases, the dehydration process leads to mixture of anhydrous phases which suddenly rehydrate to give a mixture of hydrated compounds if left in air.

The melting and/or decomposition points of **KNic·HNic·H$_2$O**, **KNic·HNic·3H$_2$O**, **NaNic·HNic·3H$_2$O**, **NaNic·HNic·2H$_2$O**, **HNic·IM**, **NaNic·DMSO·2H$_2$O** and **NaNic·DMSO·H$_2$O** are found at 294.4, 293.5, 227.6, 227.6, 275.5, 140 and 230.6 °C respectively (pure HNic= 224°C). Thus, salt co-crystal formation led to an improvement in thermal stability of about 70 °C in all cases.

Table 4. DSC and TGA data of **KNic·HNic·H$_2$O**, **KNic·HNic·3H$_2$O**, **NaNic·HNic·3H$_2$O**, **NaNic·HNic·2H$_2$O**, **HNic·IM**, **NaNic·DMSO·2H$_2$O** and **NaNic·DMSO·H$_2$O**. [T_w = water release temperatures; T_P = polymorphic transition; $T_{m/d}$ = melting/decomposition temperatures. Onset temperatures are reported. Thermal analysis data from DSC and TGA measurements of all samples].

Samples	**T_w (°C)**	**T_p (°C)**	**$T_{m/d}$ (°C)**
HNic	-	-	224.0
KNic·HNic·H$_2$O	112.8	180.0	294.4
KNic·HNic·3H$_2$O	94.0	140.0; 152.9	293.5
NaNic·HNic·3H$_2$O	95.7; 119.4	146.9; 211.9	227.6
NaNic·HNic·2H$_2$O	103.5	205.0	227.6
HNic·IM	-	218.4	275.5
NaNic·DMSO·H$_2$O	82.9	-	139.5
NaNic·DMSO·2H$_2$O	78.4; 114.1	-	230.6

Intrinsic Dissolution Rate.

It is well known that IDR is a useful indicator of potential bioavailability.[37] Dissolution tests were performed in order to compare the dissolution properties of all the compounds.

The HNic shows very poor solubility in water (reported data are variable from 5 to 15 mg/l at 20°C)[6,38] but moderate solubility in ethanol (i.e. 0.5 g/l at 20°C).[39] Its peculiar solubility prevented the measurement of the calibration curve in aqueous medium in the present work since it was lower than the UV detection limit. Thus, dissolution tests were performed in an ethanolic aqueous solution (1:1) and the resulting data are reported in **Table 7**. The IDR profiles of the salt co-crystals (in comparison with those of pure HNic and of HNic Hb) are presented in **Figure 8**. As shown, HNic and HNic Hb present comparable dissolution profiles. They dissolve more slowly than **KNic·HNic·H_2O**, **KNic·HNic·$3H_2O$** and **NaNic·HNic·$3H_2O$**. The most soluble sample was found to be **NaNic·HNic·$2H_2O$**. These results indicate that the formation of salt co-crystals provides a reliable route for modifying (in these cases improving) HNic's intrinsic dissolution rate: indeed, in the case of **NaNic·HNic·$2H_2O$** the IDR is increased by a factor of 5. This variation is comparable with that observed by forming salts of a molecule.

The measurements of the thermodynamic solubility of the co-crystals, although interesting for comparing the performances of the achieved samples, is beyond the aim of the present article.[40] However, it is also important to monitor during time the HNic concentration when powdered salt co-crystals are dissolved in a solution. Measurements of HNic concentration during time for all the samples (**Table 7**) were performed in absolute ethanol (**Figure 9**).

The most impressive improvement was achieved with **NaNic·HNic·$2H_2O$** where the HNic concentration after 72h was estimated at 24 mg/l with respect to that of pure HNic (3.5 mg/l). A

minor improvement was observed in **NaNic·HNic·3H$_2$O** where HNic concentration barely increased (14 mg/l). These data are not in contrast with IDR values. In fact, IDR measures the apparent solubility which is represented in the initial moments of measurement. The HNic concentration in **HNic·IM** also increased (22 mg/l), and the improvement is comparable to **NaNic·HNic·2H$_2$O**. The two salt co-crystals of potassium, **KNic·HNic·H$_2$O** and **KNic·HNic·3H$_2$O**, display slightly higher concentration despite being characterized by much higher IDR than pure HNic.

Table 5. IDR and HNic concentration measurements at 72h ([HNic]$_{72h}$) of **KNic·HNic·H$_2$O**, **KNic·HNic·3H$_2$O**, **NaNic·HNic·3H$_2$O**, **NaNic·HNic·2H$_2$O**, **HNic·IM**, **NaNic·DMSO·2H$_2$O** and **NaNic·DMSO·H$_2$O**.

Sample	**IDR (g/l·min)**	**[HNic]$_{72h}$ (g/l)**
HNic	0.0065	0.0035
HNic Ha	0.0059	--
HNicHb	0.00051	--
KNic·HNic·H$_2$O	0.021	0.0087
KNic·HNic·3H$_2$O	0.016	0.0079
NaNic·HNic·2H$_2$O	0.029	0.024
NaNic·HNic·3H$_2$O	0.0076	0.014
HNic·IM	0.016	0.022
NaNic·DMSO·2H$_2$O	0.0023	--
NaNic·DMSO·H$_2$O	0.0027	--

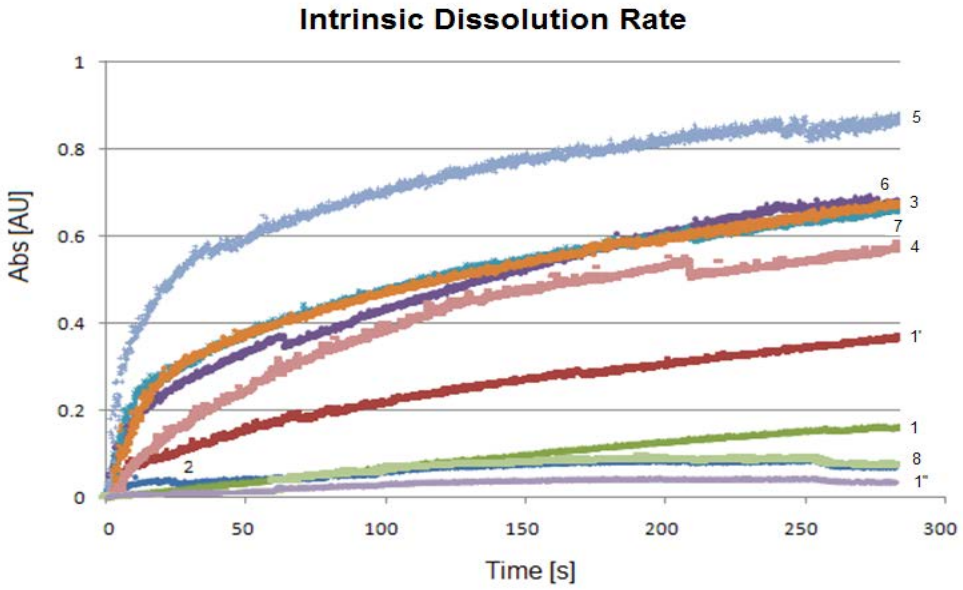

Figure 8. IDR profiles of HNic (1), HNic Ha (1'), HNic Hb (1''), **KNic·HNic·H$_2$O** (2), **KNic·HNic·3H$_2$O** (3), **NaNic·HNic·3H$_2$O** (4), **NaNic·HNic·2H$_2$O** (5), **HNic·IM** (6), **NaNic·DMSO·2H$_2$O** (7) and **NaNic·DMSO·H$_2$O** (8).

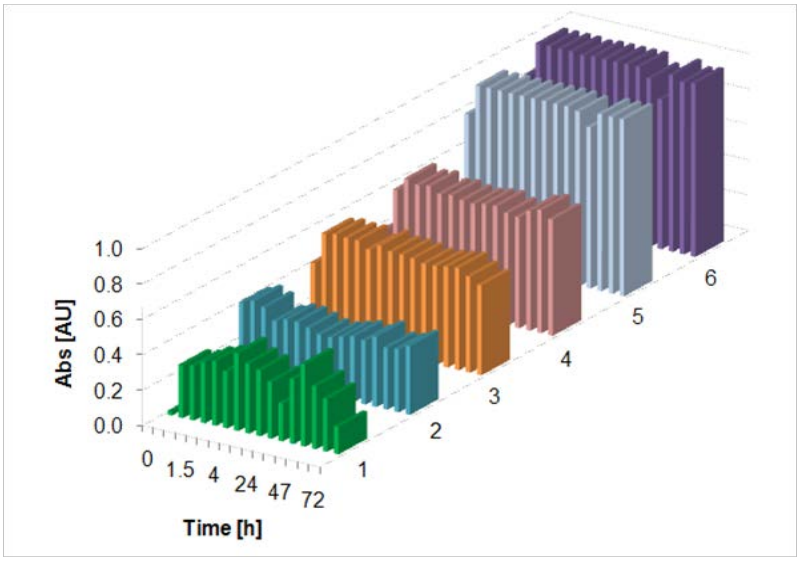

Figure 9. HNic concentration measurements at 72h ([HNic]$_{72h}$) of HNic (1), **HNic·IM** (2), **KNic·HNic·3H$_2$O** (3)**, KNic·HNic·H$_2$O** (4), **NaNic·HNic·3H$_2$O** (5), **NaNic·HNic·2H$_2$O** (6)**.**

CONCLUSIONS

HNic is a drug which is characterized by very poor solubility in water. A new series of salt co-crystals (**KNic·HNic·H_2O, KNic·HNic·3H_2O, NaNic·HNic·3H_2O, NaNic·HNic·2H_2O**) have been obtained by grinding HNic with carbonates and bicarbonates. Furthermore, a mechanochemical reaction with imidazole has provided a classic co-crystal (**HNic IM**), while, two new salts (**NaNic·DMSO·H_2O** and **NaNic·DMSO·2H_2O**) have been obtained via the salification of HNic with NaOH and subsequent kneading with DMSO. The term salt co-crystal indicates the concomitant presence, in the same unit cell, of a neutral molecule and its salt which interact via hydrogen bonding. The use of carbonates presents several advantages, since the release of CO_2 and H_2O after reaction with the API means that there are no undesired carbonates or bicarbonates in the product. All the compounds have been characterized by combined experimental techniques which are known to provide complementary information on powdered samples. These are XRPD, SSNMR (^{1}H MAS, ^{13}C and ^{15}N CPMAS, experiments), IR (ATR) and Raman spectroscopies, DSC, TGA, and IDR .

A combination of XRD and NMR data has made it possible to obtain information about the structures of powdered samples obtained by means of mechanochemical methods. SSNMR spectroscopy has been fundamental for the characterization of powdered samples which lack the long-range order necessary for XRSCD analysis.

The structures of all obtained samples are characterized by a strong $(C\text{-}O\cdots H\cdots O\text{-}C)^-$ hydrogen bond as confirmed by the large ^{1}H high frequency shift in OH signals (about 18 ppm). The peculiarity of this interaction is that it resembles a single-well hydrogen bond where the hydrogen atom lies in the middle of the contact.

All salt co-crystals show an improvement in physical properties over pure HNic in terms of increases in thermal stability and in intrinsic dissolution rate. Indeed, the formation of salt co-crystals has led to an improvement in intrinsic dissolution rate by a factor of 5 for **NaNic·HNic·3H$_2$O** and has raised the melting point for **KNic·HNic·H$_2$O** by up to 70°C.

The modification of the thermal stability, dissolution and solubility properties of an organic molecule by co-crystallization may have important implications in all areas where crystal forms are investigated and utilized, from pharmaceuticals to agro-chemicals and all of solid-state chemistry.

ASSOCIATED CONTENT

Supporting Information. Additional spectroscopic and calorimetric data for all compounds. This material is available free of charge via the Internet at http://pubs.acs.org.

AUTHOR INFORMATION

Corresponding Author

* E-mail: roberto.gobetto@unito.it. Tel: +39011-670720

REFERENCES

[1]Aakeröy, B. C.; Forbes, S.; Desper, J. *J. Am. Chem. Soc.* **2009**, *131*, 17048.
[2] Blagden, N.; de Matas, M.; Gavan, P. T.; York, P. *Adv. Drug Deliv. Rev.* **2007**, *59*, 617.
[3] Lu, J.; Rohani, S.; *Curr. Med. Chem.* **2009**, *16*, 884.
[4] Kasuga, N. C.; Umeda, M.; Kidokoro, H.; Ueda, K.; Hattori, K.; Yamaguchi, K.; *Cryst. Growth Des.* **2009**, *9*, 1494.
[5] a) Hong, J. Y.; Kim, J. K.; Song, Y. K.; Park, J. S.; Kim, C. K.; *J Control Release* **2006**, 110, 332. b) Torchilin, V. P. *J. Pharm. Res.*, **2007**, *24*, 1.
[6] Hameed, M. A.; Tarique, S. N.; J. *Drug Discov Ther*, **2013**, *1*, 13.
[7] Huang, L. F.; Tong, W. Q.; *Adv. Drug Deliv. Reviews* **2004**, *56*, 321.
[8] Vishweshwar, P.; McMahon, J. A.; Bis, J. A.; Zaworotko, M. J.; *J Pharm Sci.* **2006**, *95*, 499.
[9] Aakeröy, C. B.; Salmon, D. J.; *CrystEngComm***2005**, *7*, 439.
[10] Qiao,N.; Li, M.; Schlindwein, W.; Malek, N.; Davies, A.; Trappitt, G. *Int. J. Pharm*. **2011**, *419*, 1.
[11] Issa, N.; Karamertzanis, P. G.; Welch, G. W. A.; Price, S. L. *Cryst. Growth. Des.* **2009**, *9*, 442.
[12] Vogt, F. G.; Clawson, J. S.; Strohmeier, M.; Edwards, A. J.; Pham, T. N.; Watson, S. A. *Cryst. Growth Des.* **2009**, *9*, 921.
[13] Berry, D. J.; Seaton, C. C.; Clegg, W.; Harrington, R. W.; Coles, S. J.; Horton, P. N.; Hursthouse, M. B.; Storey, R.; Jones, W.; Fri, T.; Blagden N. *Cryst. Growth Des.* **2008**, *8*, 1697.
[14] Braga, D.; Grepioni, F.; Maini, L.; Prosperi, S.; Gobetto, R.; Chierotti, M. R. *Chem. Commun*. **2010**, *46*, 7715.
[15] Brittain, H. G. *J. Pharm. Sci.* **2013,** *102*, 311..
[16] Gaglioti, K.; Chierotti, M. R.; Grifasi, F.; Gobetto, R.; Griesser, U.; Hasa, D.; Voinovich, D. *CrystEngComm*, **2014**, *16*, 8252.
[17] WHO (World Health Organisation), The control of schistosomiasis: Second report of the WHO Expert Committee **1993**.
[18] Andersen,. K. V; Larsen, S.; Alhede, B.; Gelting, N.; Buchardt, O.; *J. Chem. Soc, Perkin Trans.* **1989**, *2*, 1443.
[19] Harriss, B. I.; Wilson, C.; Evans, I. R. *Acta Crystallogr. Sect. C-Struct. Chem.* **2014**, *70*, 758
[20] Sanphui, P.; Kumar, S. S.; Nangia, A. *Cryst. Growth Des.* **2012**, *12*, 4588.
[21] A patent including the four salt co-crystals have been registered on the 4th August 2014 (registered number TO2014A000630).
[22] Chierotti, M. R.; Gaglioti, K.; Gobetto, R.; Braga, D.; Grepioni, F.; Maini, L. *CrystEngComm* **2013**, *15*, 7598.
[23] Braga, D.; Grepioni, F.; Polito, M.; Chierotti, M. R.; Ellena, S.; Gobetto, R. *Organometallics* **2006**, *25*, 4627.
[24] Braga, D.; Maini, L.; Fagnano, C.; Taddei, P.; Chierotti, M. R.; Gobetto, R. *Chem. Eur. J.* **2007**, *13*, 1222.
[25] Friščić, T. *Chem. Soc. Rev.* **2012**, ***41***, 3493.
[26] Braga, D.; Maini, L.; Grepioni, F. *Chem. Soc. Rev.* **2013**, *42*, 7638.
[27] De Villiers M. M.; Mahlatji M. D., van Tonder E. C., Malan S. F., Lötter A. P., Liebenberg W., *Drug Dev Ind Pharm.* **2004**, *30*, 581.
[28] SHELXL97, Sheldrick, G. M. University of Gçttingen, Gçttingen (Germany), **1997**
[29] Powder Cell, Version 2.3, Kraus, W.; Nolze, G. Berlin (Germany), **1999**
[30] Van Rossum, B. J.; de Groot, C. P.; Ladizhansky, V.; Vega, S.; de Groot, H.J.M. *J. Am. Chem. Soc*. **2000**, *122*, 3465.
[31] Antzutkin, O. N.; Shekar, S. C.; Levitt, M. H.; *J. Magn. Reson. Ser. A* **1995**, *115*, 7-19.
[32] Antzutkin, O. N.; Lee, Y. K.; Levitt, M. H. *J. Magn. Reson*. **1998**, *13*5, 144-155.
[33] Stahl, P. H.; Wermuth, C. G. *Handbook of Pharmaceutical salts: properties, selection and use*, Wiley-VCH, Freiburg im Breisgau **2008**, 19.
[34] Chierotti, M. R.; Gobetto, R. *"Solid-State NMR Studies on Supramolecular Chemistry"*, John Wiley & Sons, **2012**.
[35] Hickman, B. S.; Mascal, M.; Titman, J. J.; Wood, I. G. *J. Am. Chem. Soc.* **1999**, *121*, 11486.
[36] Bettini, R.; Menabeni, R.; Tozzi, R.; Pranzo, M. B.; Pasquali, I.; Chierotti, M. R.; Gobetto, R.; Pellegrino, L. *J. Pharm. Sci.* **2010**, *99*, 1855.
[37] Issa, M. G.; Ferraz, H. G. *Dissolut. Technol.* **2011**, *18*, 6.
[38] Devarakonda, B.; Hill, R. A.; Liebenberg, W.; Brits, M.; De Villiers, M. M. *Int. J. Pharm*. **2005**, *304*, 193.
[39] *Cayman Chemical Company*, Registration number CAS: 50-65-7.
[40] Good, D. J.; Rodriguez-Hornedo, N. *Cryst. Growth Des.* **2009**, *9*, 2252.

For Table of Contents Use Only

Using Salt Co-Crystals to Improve the Solubility of Niclosamide

Francesca Grifasi,[†] Michele R. Chierotti,[†] Katia Gaglioti,[†] Roberto Gobetto,[†] Lucia Maini,[‡] Dario Braga,[‡] Elena Dichiarante,[§] and Marco Curzi[§]*

† Dipartimento di Chimica I.F.M., Università di Torino, Via Giuria 7, 10125 Torino, Italy

‡ Dipartimento di Chimica G. Ciamician, Universitàdegli Studi di Bologna, Via Selmi 2, 40126 Bologna, Italy

§ PolyCrystalLine s.r.l., via F. S. Fabri 127/1, 40059 Medicina, Italy

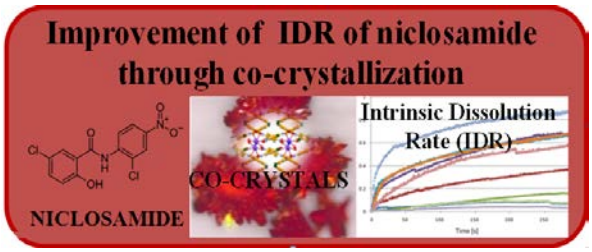

This paper sees us report the solvent-free synthesis and characterization of five new co-crystals and two salts of niclosamide, an antihelmintic API with poor intrinsic dissolution rate. All samples have been characterized through solid-state techniques such as SSNMR, XRPD, IR and Raman. The formation of salt co-crystals reveal to be a reliable method to improve the niclosamide intrinsic dissolution rate.

Supporting Information

Using Salt Co-Crystals to Improve the Solubility of Niclosamide

Francesca Grifasi,[†] Michele R. Chierotti,[†] Katia Gaglioti,[†] Roberto Gobetto,*[†] Lucia Maini,[‡] Dario Braga,[‡] Elena Dichiarante,[§] and Marco Curzi[§]

† Dipartimento di Chimica I.F.M., Università di Torino, Via Giuria 7, 10125 Torino, Italy

‡ Dipartimento di Chimica G. Ciamician, Universitàdegli Studi di Bologna, Via Selmi 2, 40126 Bologna, Italy

§ PolyCrystalLine s.r.l., via F. S. Fabri 127/1, 40059 Medicina, Italy

Figures S1: XRPD patterns of all prepared samples

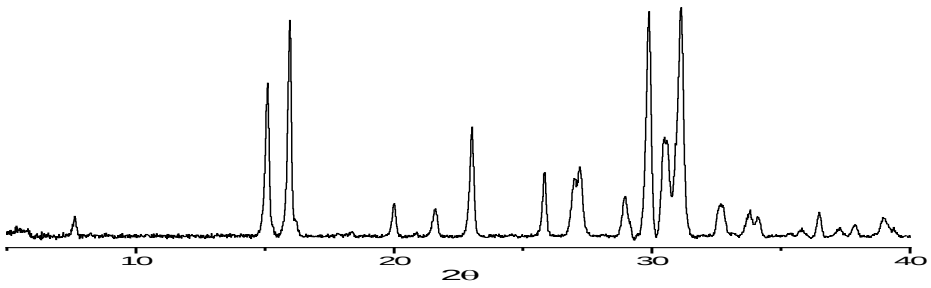

a) Experimental pattern of pure Niclosamide (HNic).

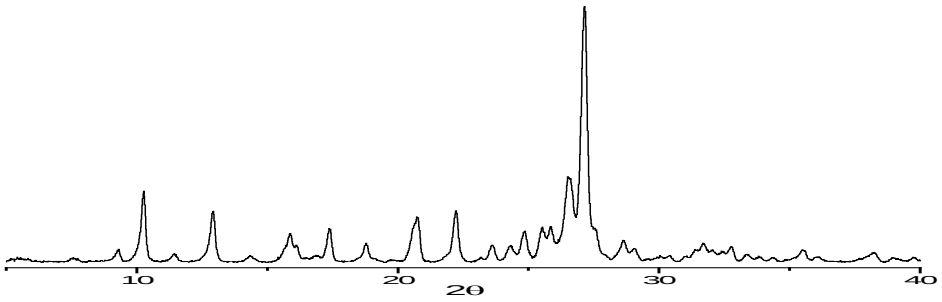

b) Experimental pattern of HNic Ha.

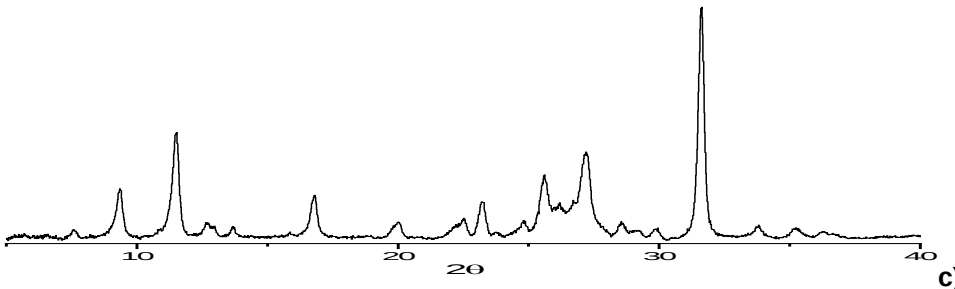

c) Experimental pattern of HNic Hb.

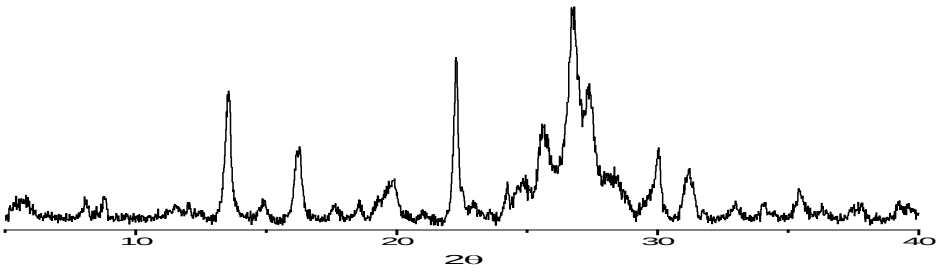

d) Experimental pattern of **KNic·HNic·H_2O**.

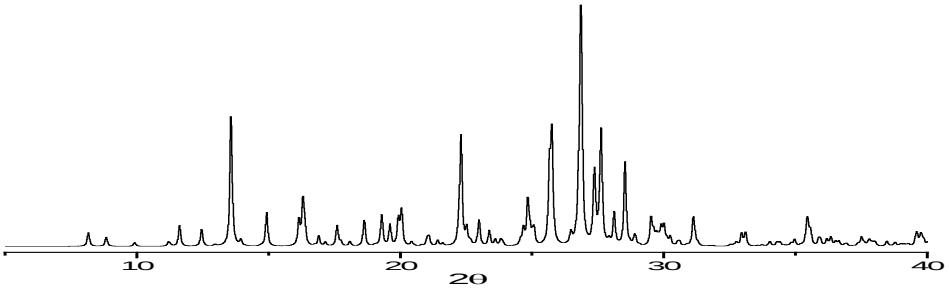

e) Experimental pattern of **KNic·HNic·$3H_2O$**.

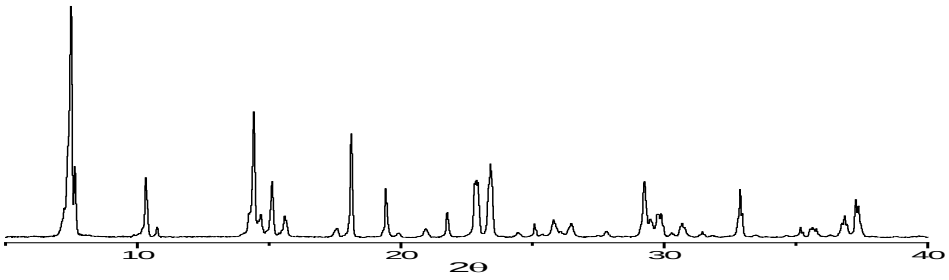

f) Experimental pattern of **NaNic·HNic·2H$_2$O**.

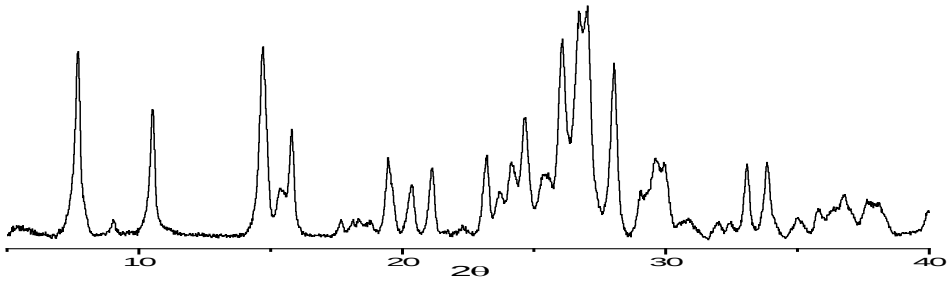

g) Experimental pattern of **NaNic·HNic·3H$_2$O**.

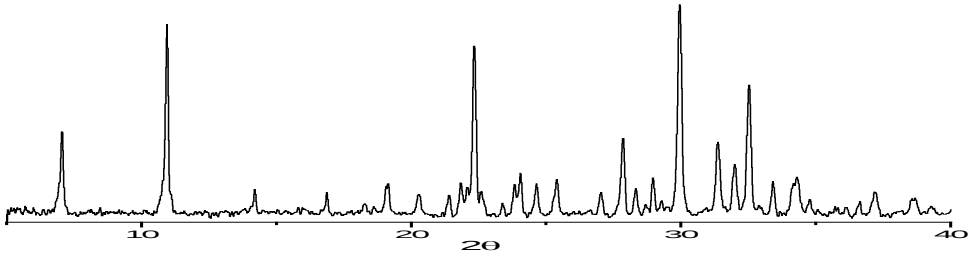

h) Experimental pattern of **NaNic·DMSO·2H$_2$O**.

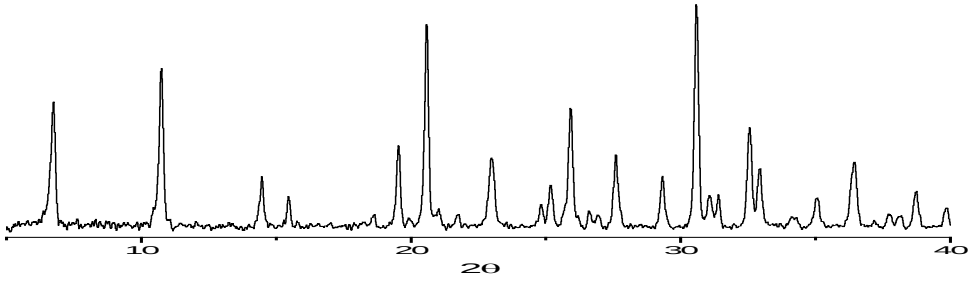

i) Experimental pattern of **NaNic·DMSO·H$_2$O**.

Figures S2: Raman spectra of all prepared compounds.

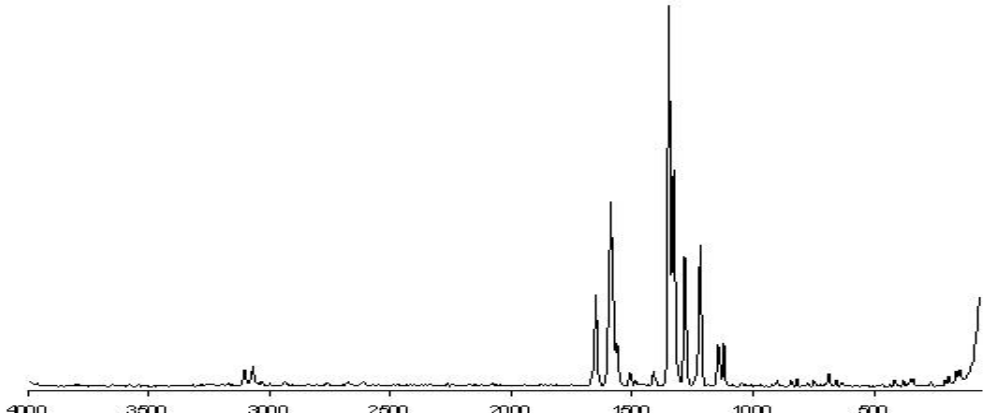

a) Raman spectrum of pure HNic.

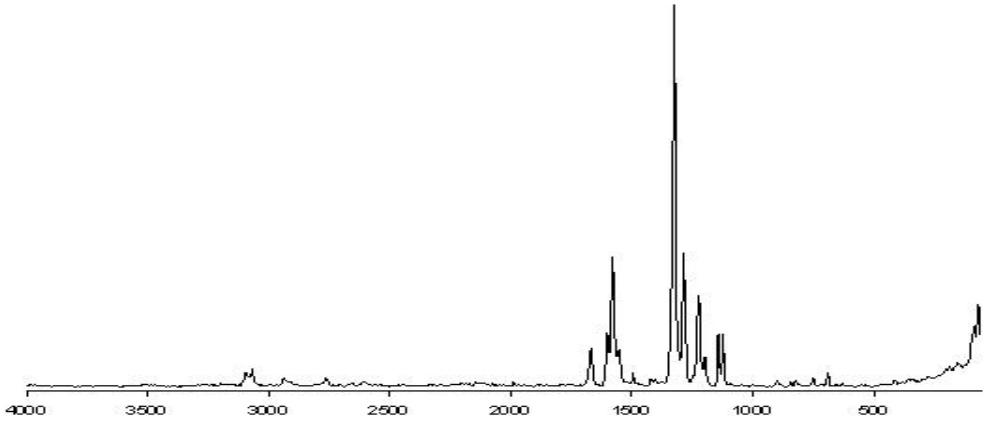

b) Raman spectrum of HNic Ha.

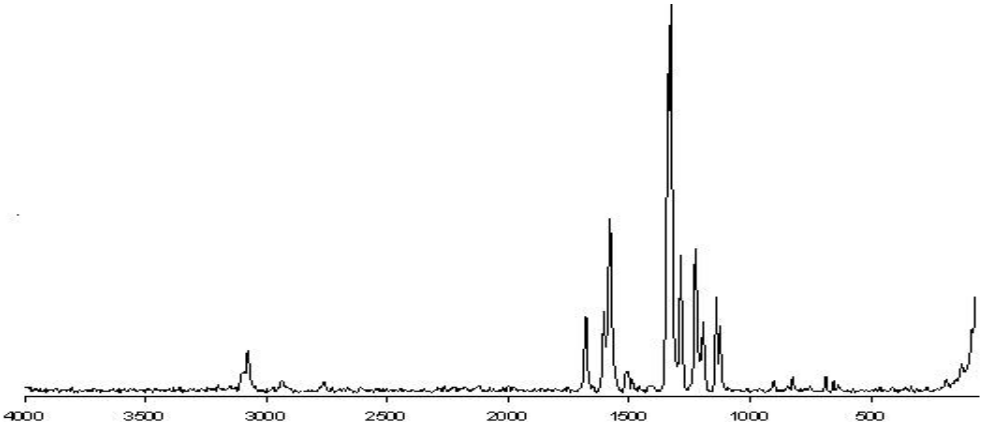

c) Raman spectrum of pure HNic Hb.

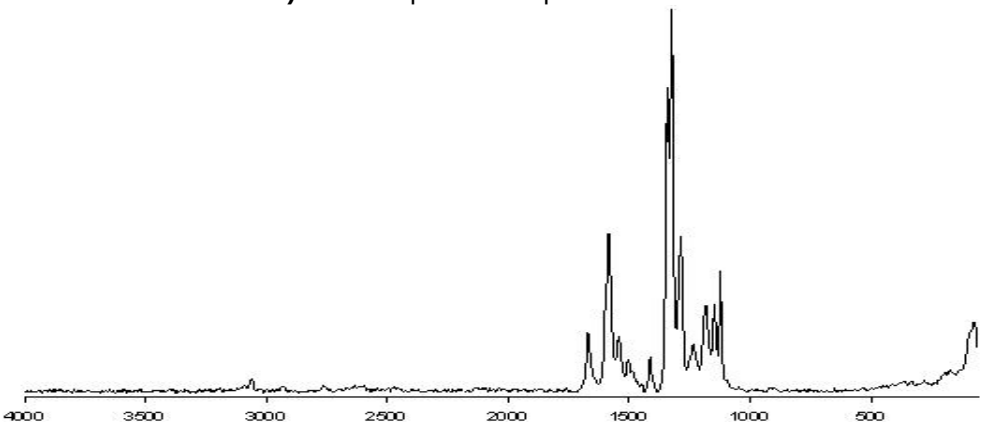

d) Raman spectrum of **KNic·HNic·H_2O**.

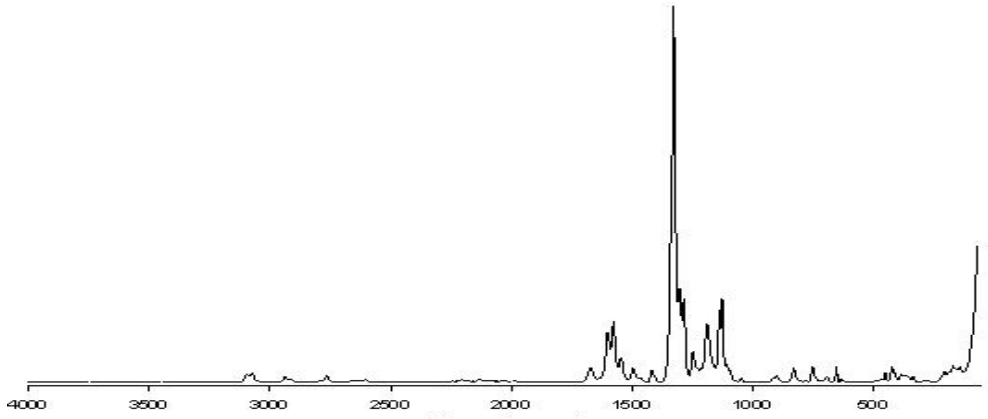

e) Raman spectrum of **KNic·HNic·3H$_2$O**.

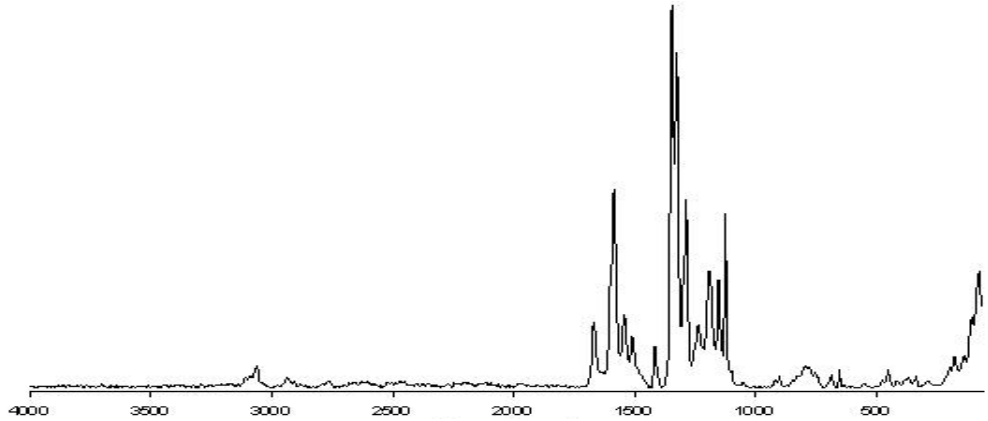

f) Raman spectrum of **NaNic·HNic·2H$_2$O**

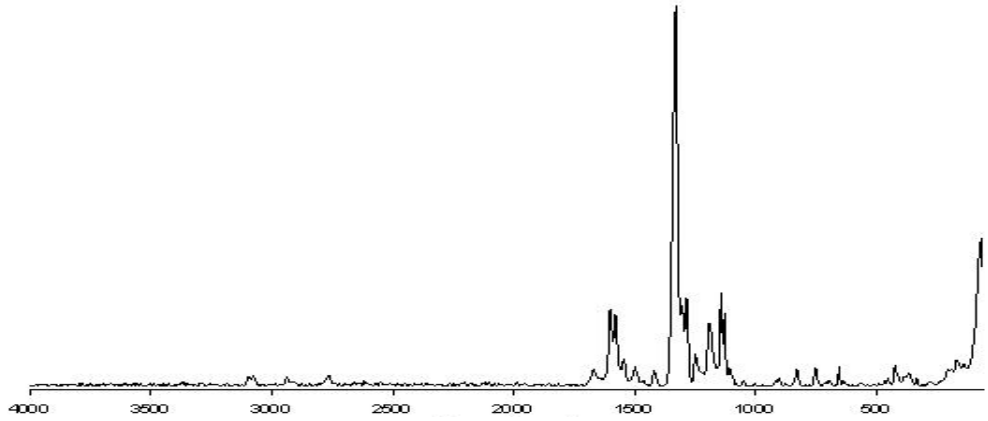

g) Raman spectrum of **NaNic·HNic·3H$_2$O**.

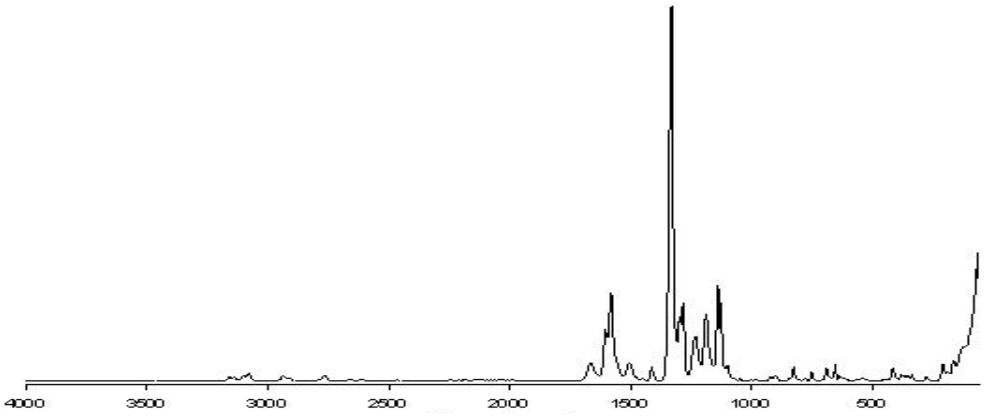

h) Raman spectrum of **HNic·IM**.

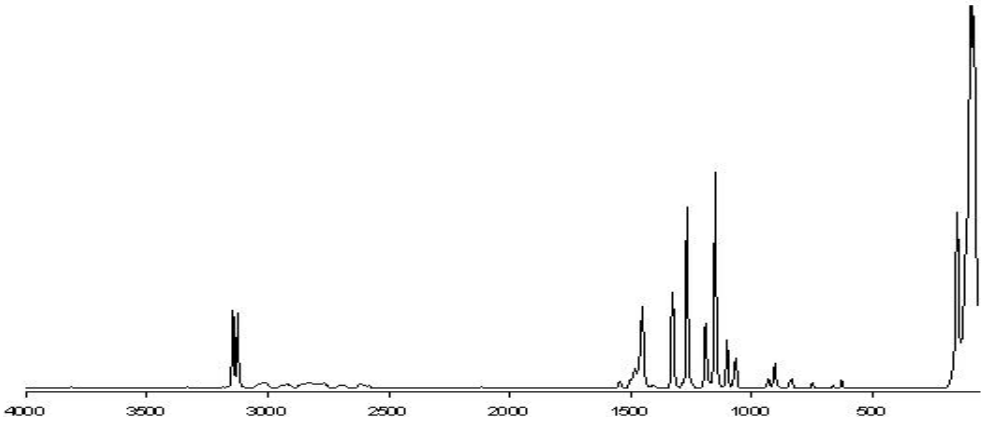

i) Raman spectrum of pure Imidazole (IM).

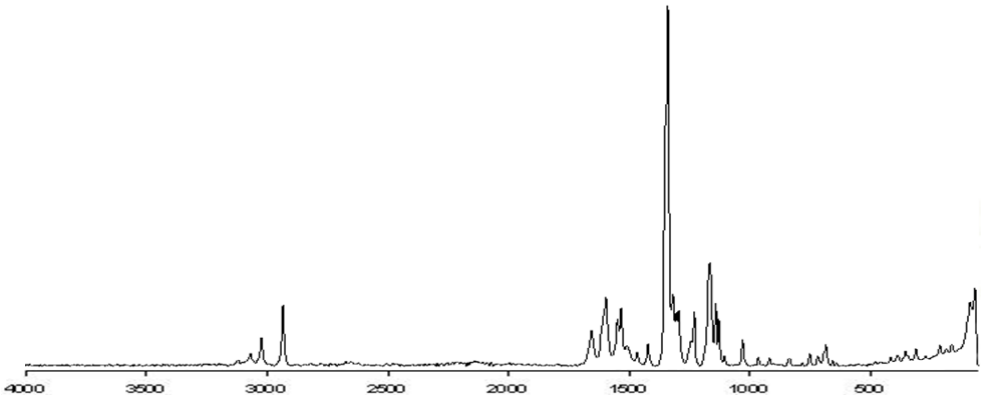

l) Raman spectrum of **NaNic·DMSO·2H$_2$O**.

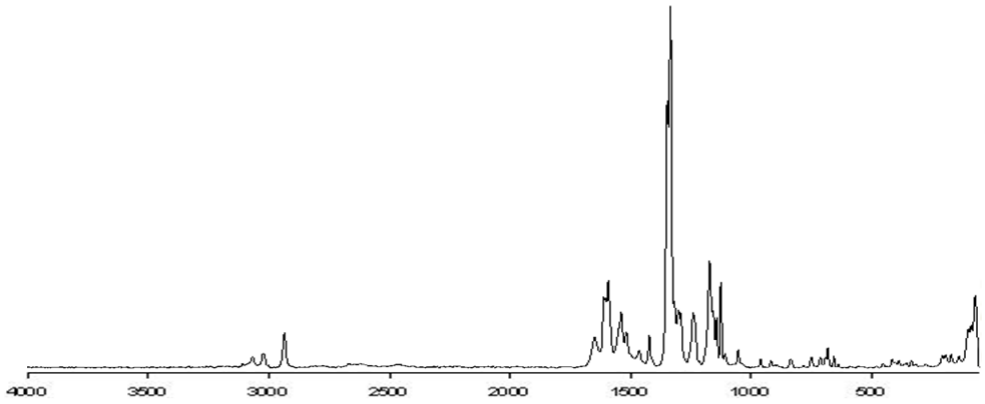

m) Raman spectrum of **NaNic·DMSO·3H$_2$O**.

Figures S3: IR (ATR) spectra of all prepared compounds

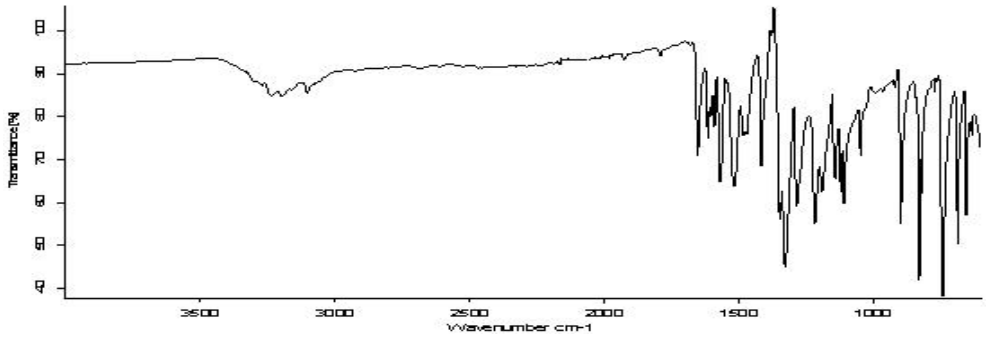

a) IR (ATR) spectrum of pure Niclosamide.

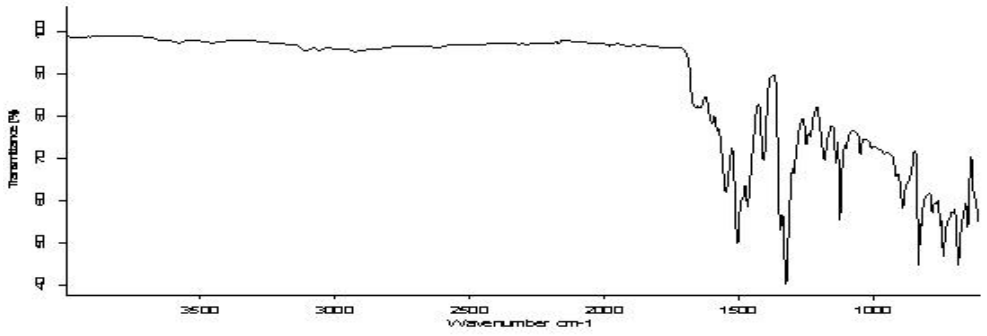

b) IR (ATR) spectrum of **KNic·HNic·H_2O**.

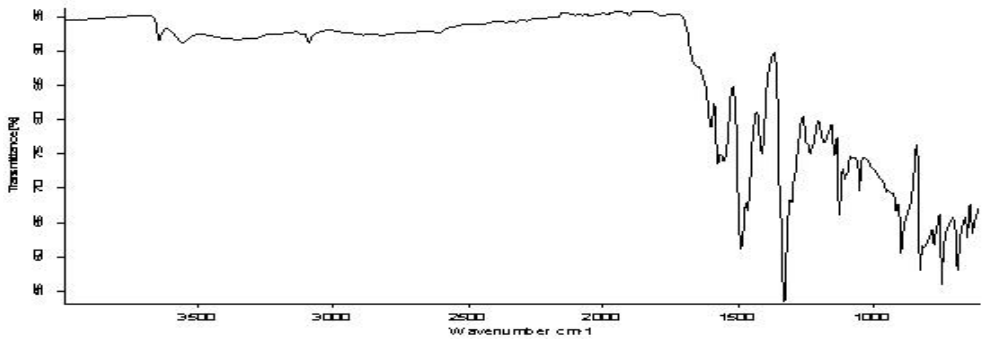

c) IR (ATR) spectrum of **KNic·HNic·3H_2O**.

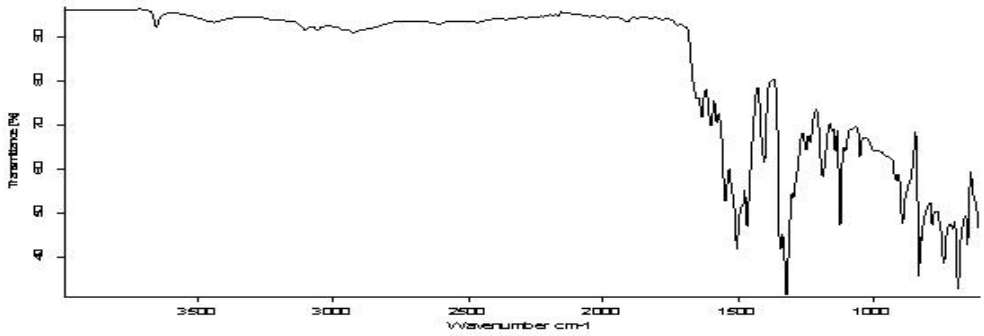

d) IR (ATR) spectrum of **NaNic·HNic·2H_2O**.

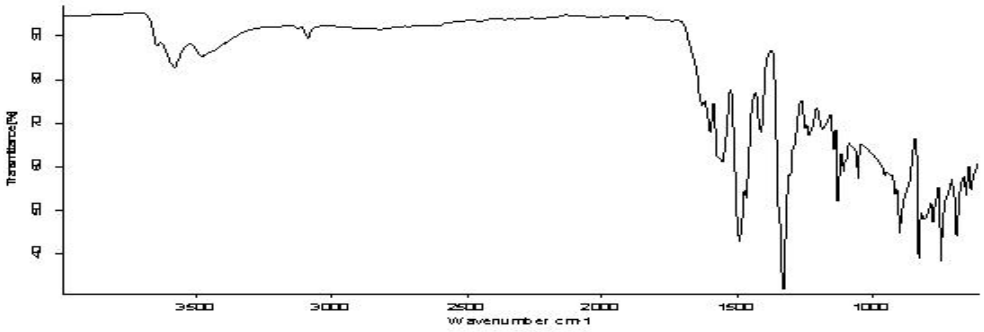

e) IR (ATR) spectrum of **NaNic·HNic·3H_2O**.

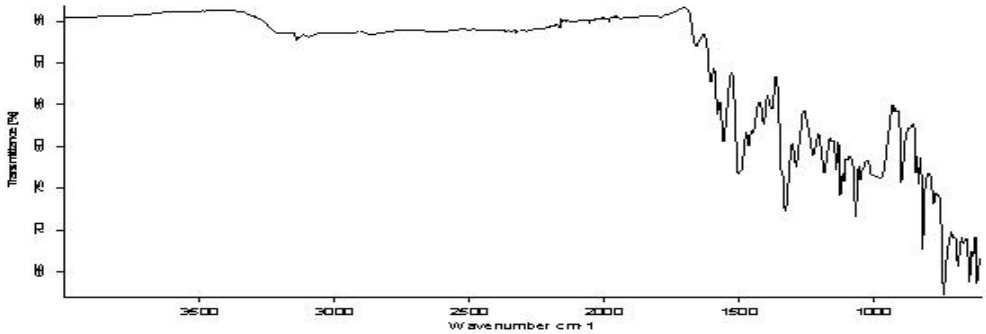

f) IR (ATR) spectrum **HNic·IM**.

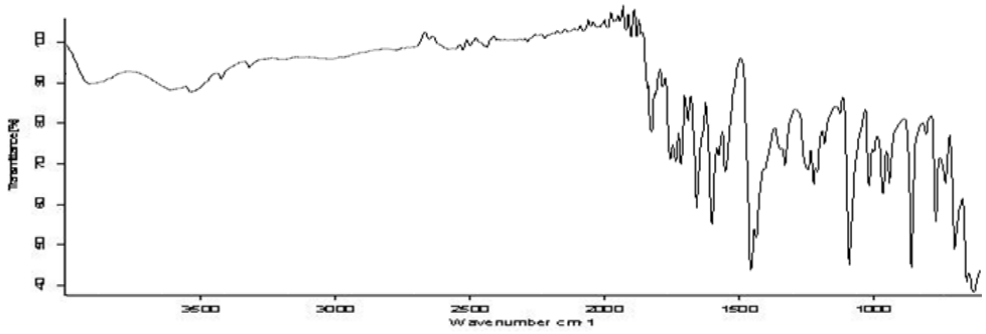

g) IR (ATR) spectrum **HNic·DMSO·2H$_2$O**.

Figures S4: Calorimetric and Thermogravimetric curves.

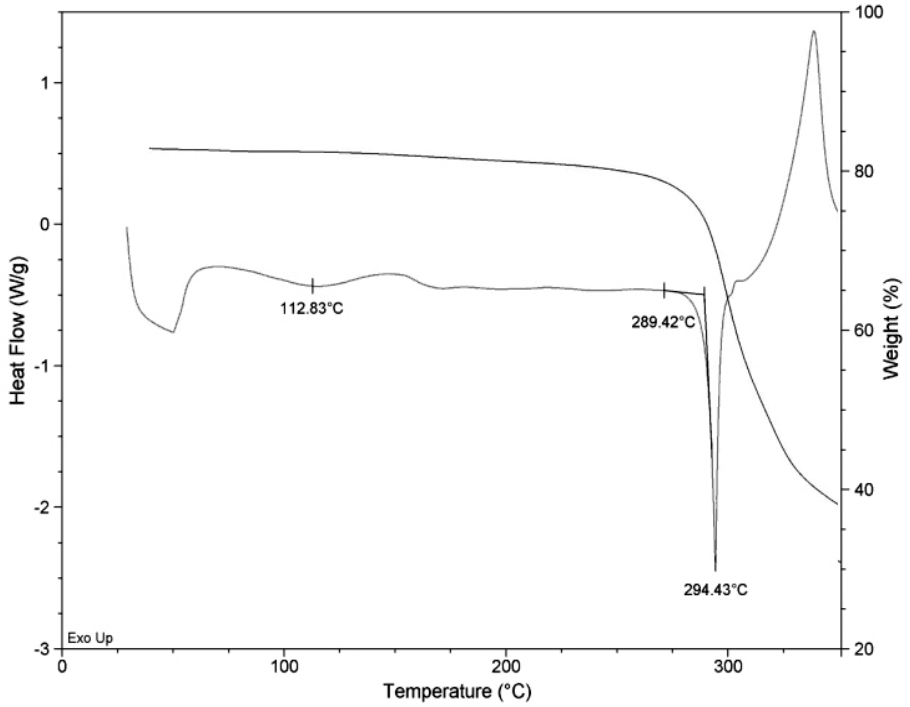

a) DSC and TGA curves of **KNic·HNic·H_2O**

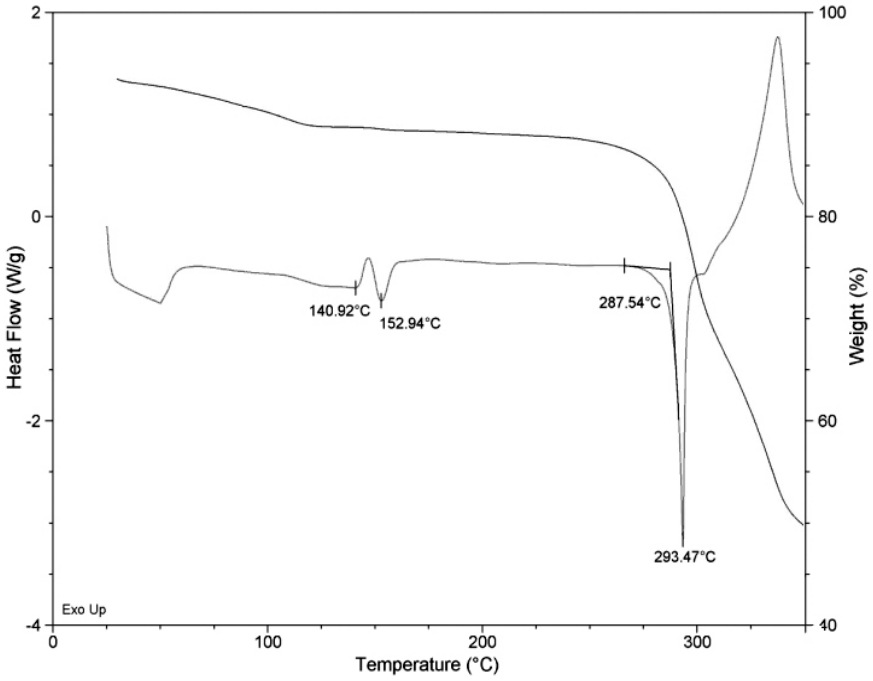

b) DSC and TGA curves of of **KNic·HNic·3H_2O.**

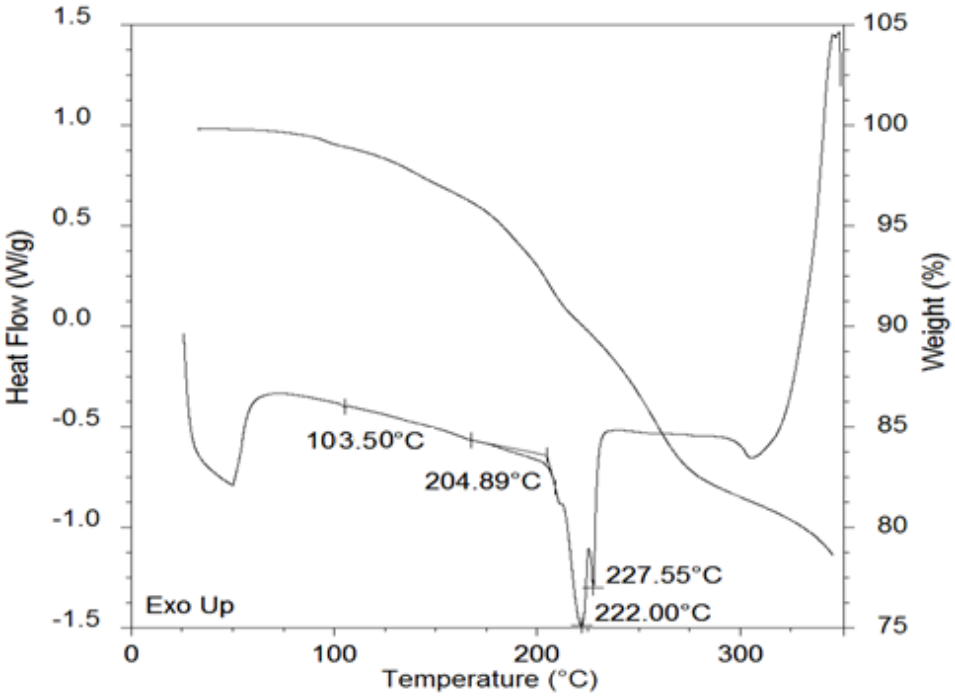

c) DSC and TGA curves of **NaNic·HNic·2H_2O**

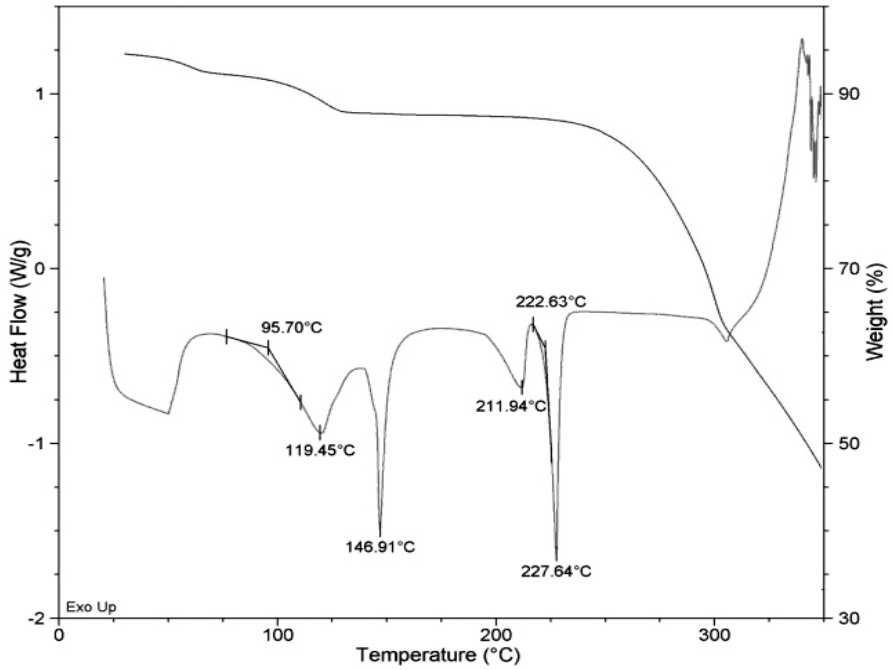

d) DSC and TGA curves of of **NaNic·HNic·3H_2O.**

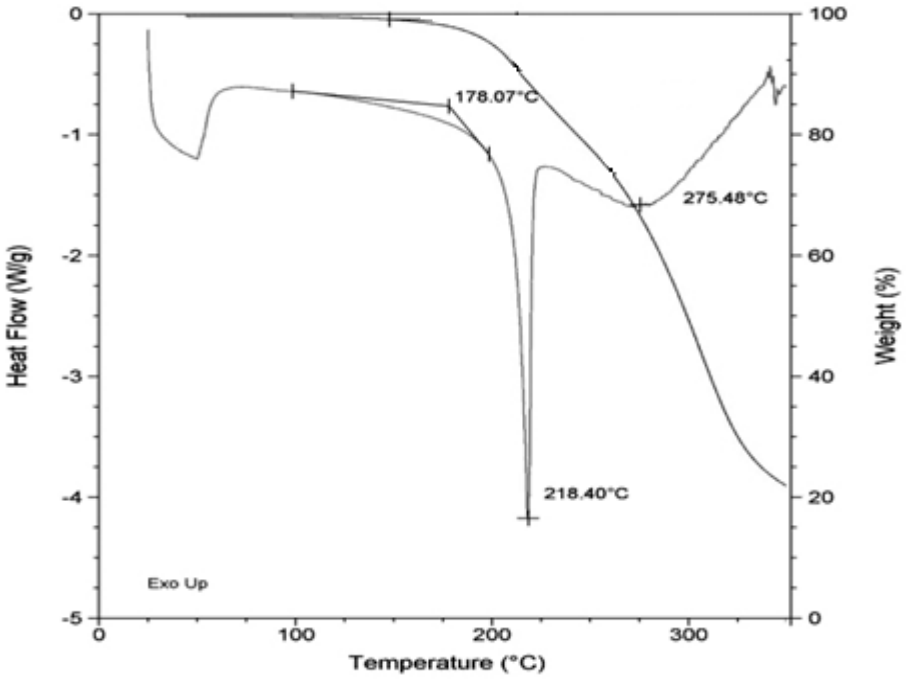

e) DSC and TGA curves of **HNic·IM**

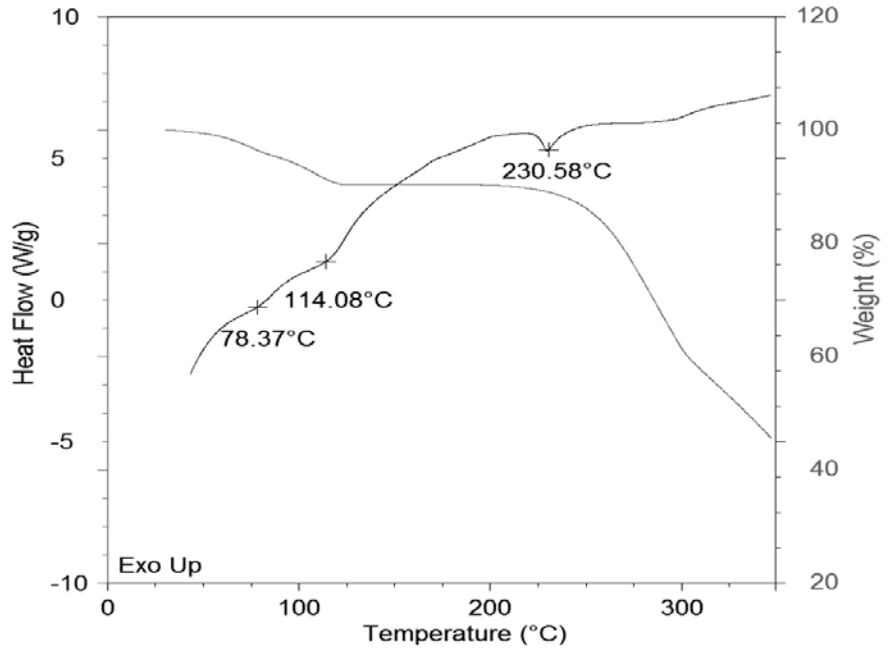

f) DSC and TGA curves of NaNic·**DMSO·2H_2O**

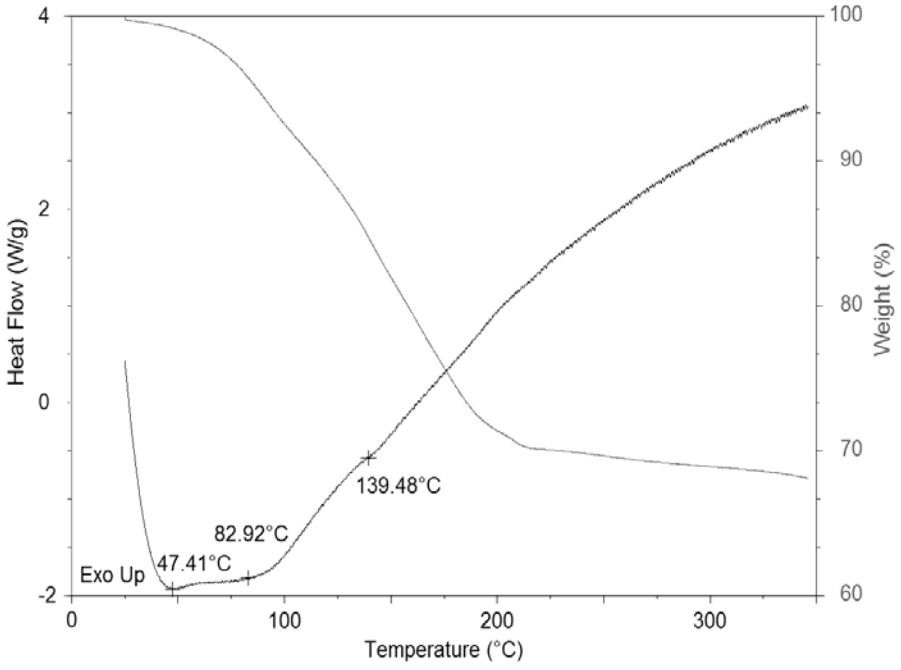

g) DSC and TGA curves of **NaNic·DMSO·H_2O**.